

# A calculation method of phenotypic traits based on three-dimensional reconstruction of tomato canopy



Tianyu Zhu<sup>a</sup>, Xiaodan Ma<sup>a</sup>, Haiou Guan<sup>a,b,\*</sup>, Xia Wu<sup>c</sup>, Feiyi Wang<sup>a</sup>, Chen Yang<sup>a</sup>, Qiu Jiang<sup>a</sup>

<sup>a</sup> College of Information and Electrical Engineering, Heilongjiang Bayi Agricultural University, Da Qing 163319, China

<sup>b</sup> Key Laboratory of Low-carbon Green Agriculture in Northeastern China, Ministry of Agriculture and Rural Affairs, Daqing 163319, China

<sup>c</sup> College of Landscape and Horticulture, Heilongjiang Bayi Agricultural University, Da Qing 163319, China

## ARTICLE INFO

## ABSTRACT

### Keywords:

Tomato canopy  
Machine vision  
3D reconstruction  
Phenotypic traits  
Calculation method

Accurate and rapid acquisition of tomato canopies' phenotypic traits was significant for variety breeding, cultivation, and scientific management. Manual measurements were time-consuming, laborious, and error-prone. The large devices in the field were lack of mobility, while the single perspective was limited by the environment's obstruction, making it challenging to achieve high-throughput detection of tomato plants' phenotypes. Therefore, a method for high-throughput detection of tomato canopy's phenotypic traits was proposed based on three-dimensional (3D) structure reconstruction with multi-views. First, the tomato variety named Dongnong 708 was set as an experimental object. The acquisition platform was constructed using three Kinect 2.0 sensors to acquire a full range point cloud of tomato canopy at crucial growth stages, including the initial flowering stage, fluorescence, and primary fruit stage. Second, the background and interference noises were removed by Conditional filtering and Statistical Outlier Removal (SOR) filtering. Then, its structural characteristic points were extracted, and spatial position was registered by combining with Intrinsic Shape Signatures (ISS) and Iterative Closest Point (ICP) algorithms. In addition, the 3D-Normal Distributions Transform (NDT) algorithm was used to realize accurate registration of three perspectives' point clouds. Compared with NDT and ICP algorithms, the average error of the proposed methods here was 0.027, reduced by 0.02 and 0.04, respectively. Finally, the contour of tomato canopy was extracted using the AlphaShape algorithm. Based on the reconstructed result, plant height, canopy width, and leafstalk angle, were calculated. The results showed that the correlation coefficients were 0.9615, 0.809 and 0.9014 between the calculated values and measured values. The average errors were 1.38 cm, 5.1° and 1.92 cm, respectively. The methods proposed in the paper could be used as a rapid detection method for quantitative indexes of the phenotypic traits for the tomato canopy and provide technical support for breeding, scientific cultivation, and environmental regulation.

## 1. Introduction

Tomato, with great nutritional and economic value, is one of the most common greenhouse crops cultivated in the world (Li et al., 2020a, b). In tomato cultivation management, due to the complex morphological structure of tomato growth (Dong et al., 2010; Sun et al., 2019; Shin et al., 2021), the most common measurement method of its phenotypic traits was done mainly by traditional manual measurements (Yuan et al., 2012). It was still one of the production processes with low operation

efficiency and large workforce input in tomato crop breeding and planting.

At present, many achievements have been made in the visualization of crop organs and plants and the calculation of plant type characteristics such as Rice (Burgess et al., 2017), Wheat (Li et al., 2020a, b), Maize (Liu et al., 2021a), Soybean (Guan et al., 2019). Phenotypic research on tomato plants mainly focused on biomass production and distribution during growth stages (Huo et al., 2021; Zhu et al., 2021; Zhao et al., 2021), but the visualization of tomato plants and calculation of

**Abbreviations:** 3D, Three-dimensional; 3D-NDT, Three dimensional - Normal Distribution Transform; Ca<sub>3</sub>(PO<sub>4</sub>)<sub>2</sub>, Calcium Phosphate; CPD, Coherent Point Drift; K<sub>2</sub>SO<sub>4</sub>, Potassium sulphate; ICP, Iterative Closest Point; ISS, Intrinsic Shape Signatures; LiDAR, Laser Radar; NDT, Normal Distribution Transform; RGB, Red, Green, and Blue; RGB-D, Red, Green, Blue and Depth; R, Correlation Coefficient; R<sup>2</sup>, Coefficient of Determination; SOR, Statistical Outlier Removal; TOF, Time of Flight.

\* Corresponding author at: College of Information and Electrical Engineering, Heilongjiang Bayi Agricultural University, Da Qing 163319, China.

E-mail addresses: [bynd\\_zty@163.com](mailto:bynd_zty@163.com) (T. Zhu), [mxd@cau.edu.cn](mailto:mxd@cau.edu.cn) (X. Ma), [gho@cau.edu.cn](mailto:gho@cau.edu.cn) (H. Guan), [wuxiaxia\\_2005@163.com](mailto:wuxiaxia_2005@163.com) (X. Wu), [bynd\\_wfy@163.com](mailto:bynd_wfy@163.com) (F. Wang), [bynd\\_yc@163.com](mailto:bynd_yc@163.com) (C. Yang), [bynd\\_jq@163.com](mailto:bynd_jq@163.com) (Q. Jiang).

<https://doi.org/10.1016/j.compag.2022.107515>

Received 17 July 2022; Received in revised form 18 November 2022; Accepted 18 November 2022

Available online 26 November 2022

0168-1699/© 2022 Elsevier B.V. All rights reserved.

phenotypic traits have not been thoroughly researched. Researchers in relevant fields mainly focused on developing versatile and high-throughput automated phenotype acquisition technologies to facilitate management and breeding efforts. Schunck et al. conducted full-time and space-time data collection on corn and tomatoes to construct a complete 3D point cloud data set of crops (Schunck et al., 2021). Rose et al. used motion structure (SFM) and multi-view stereo structure (MVS) methods to reconstruct tomatoes from two-dimensional(2D) images (Rose et al., 2015). DaSilva et al. measured the leaf area and fruit tree volume accurately based on a 3D reconstruction of apple trees (Da Silva et al., 2014). Rouzbeh Kargar et al. used near-earth lidar to obtain the population point cloud model of various horticultural trees. On this basis, they realized the segmentation of the tree canopy and calculated leaf area index of multiple plants (Rouzbeh Kargar et al., 2019). 3D reconstruction techniques with color information could be used in phenotypic studies to obtain completer phenotypic traits of plants. So, the limitation of lack of depth information in 2D imaging could be avoided (Gao et al., 2022; Forero et al., 2022). Automated measurement of tomato plant traits could be achieved. While in the large greenhouse production area, the scheme of using the unmanned aerial vehicle (UAV) to obtain the phenotypic traits of facility crops was interfered with by the shelter equipment, which was difficult to implement well. LiDAR, a large multi-spectral laser scanner, and other devices could be used to obtain leaf area index, projection area, biomass content, and other phenotypic traits which couldn't be measured manually (Li et al., 2019). Most of the above devices were expensive and needed configuring the appropriate auxiliary equipment and lines for stably using. Thus, such devices were difficult to be used in the actual production of tomato plants widely (Yu et al., 2019). In contrast, the Kinect 2.0 sensor based on the TOF principle was able to acquire color images and depth information. It was also portable, cheap, and easily integrated into devices such as near-Earth mobile platforms and unmanned ground vehicles.

This was conducive to expanding the Kinect sensor in the practical application of the production of smart facility agronomy (Caruso et al., 2017; Condotta et al., 2020). With the application of the Kinect 2.0 sensor, it provided technical support for the study of reconstructing the 3D structure of the tomato canopy with color information and accurately obtaining the multidimensional phenotypic traits of the plant. It also provided the primary conditions for applying these ecological and morphological traits for evaluating stress, yield, breeding, cultivation, and management. Therefore, three Kinect 2.0 sensors were used to construct a multi-view acquisition system to obtain heterogeneous data of tomato canopy's color image and depth information. These data were used to establish the high-throughput automated detection method for tomato canopy's phenotypic traits through the in-depth fusion of plant color images. First, the ISS + ICP algorithm was used for rapid rough registration of tomato canopy's point clouds at different perspectives. The multi-perspective point clouds could obtain a better initial spatial pose. Then, for quick and accurate registration of point clouds, the 3D-NDT algorithm was used to achieve the fusion and splicing of the tomato canopy's point clouds at different perspectives. On this basis, the 3D structure model of the tomato canopy with color information was reconstructed. The phenotypic traits of tomato canopy were also calculated to meet the actual needs of determining the tomato plants' nutrition, growth, and biomass and predicting yield.

## 2. Experimental materials and data collection

### 2.1. Experimental materials

The experimental design of this study was based on the effect of tillered onion on the growth index of tomato plants in each growth stage to construct a method for rapid characterization of the tomato physiological index. Tomato planting and canopy information acquisition work was conducted in Daqing Urban Agricultural Demonstration Park in

Heilongjiang Province. In this study, tomatoes planted in pots to investigate high-throughput methods for detecting strain and physiological traits. By effectively controlling the soil, fertilizer and water conditions in the pots, the relationship between the changing characteristics of the tomato plants' physiological indicators, the accompanying tiller onion treatment, the changing characteristics of the tomatoes' physiological indicators, and soil nutrient transformation could be investigated simultaneously. The Dongnong 708 tomato was selected as the experimental object. This variety belongs to the indeterminate growth type, with the characteristics of early maturity and high quality. Its growth was medium-strong, with large plant width, and the average seedling age was 60 days (Wu et al. 2016). In the experiment, potted tomato seedlings were planted in plastic buckets with a diameter of 34 cm and a height of 23 cm at the five-leaf with one-center stage. The tomato continuous cropping soil in the greenhouse for more than four years was taken during colonization. According to calcium phosphate ( $\text{Ca}_3(\text{PO}_4)_2$ ) 0.55 g  $\text{kg}^{-1}$  and potassium sulfate ( $\text{K}_2\text{SO}_4$ ) 0.67g  $\text{kg}^{-1}$ , the fertilizer and soil were mixed and put into pots, with 7.5 kg soil in each pot.

Tomato seedlings were raised on March 28th and were separated on April 22nd. On May 22, the tomato was planted in plastic buckets according to the treatment number, and performed regular field management after planting. The experiment divided into six treatments. The numbers and corresponding treatments are shown in Table 1:

Point cloud data, image information, and phenotypic data collected at 20d (initial flowering stage, June 12th), 30 d (florescence, June 22nd), and 40 d (primary fruit stage, July 3rd). The basic configuration of the computer, which processed the 3D point cloud data was equipped with: Core i5-6500 CPU, RAM of 16.0 GB, and graphics card of HD530 as well as solid-state hard disk of KINGSTONSA400S37.

### 2.2. The process of the experiment

Based on the above experimental design, the overall process of 3D reconstruction of the tomato canopy and calculation of phenotypic traits is shown in Fig. 1.

First, a multi-source data acquisition platform was constructed based on Kinect 2.0 sensor to obtain the point cloud data of the target crop with color information,

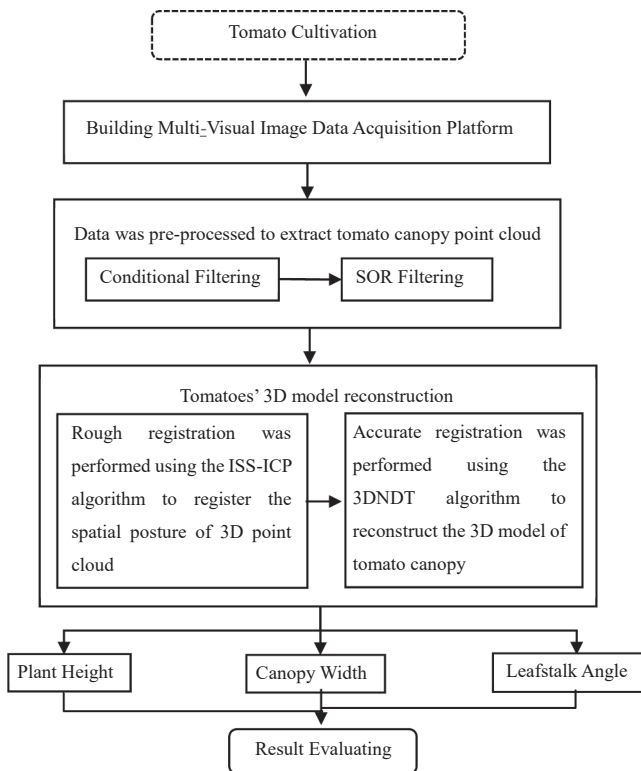
Second, biconditional filtering and SOR filtering algorithms were used to extract tomato canopy from redundant original point cloud data.

Third, the ISS-ICP and 3DNDT algorithms we used to realize the registration and fusion of multi-view canopy point clouds.

Fourth, the AlphaShape method was used to accurately obtain the clear boundary of the tomato canopy. Then, the phenotypic traits, including plant height, canopy width, and leafstalk angle, were

**Table 1**  
Experimental pot number and corresponding treatment.

Experimental control group serial numbers	Serial numbers of treatments	Whether associated with tillered onion	The rate of nitrogen fertilizer
1	CK1	No	No
	CK2	Yes	No
2	T1	No	0.33 g $\text{kg}^{-1}$
	T2	Yes	0.33 g $\text{kg}^{-1}$
3	T3	No	0.33 g $\text{kg}^{-1}$
	T4	Yes	0.33 g $\text{kg}^{-1}$



calculated.

Finally, the 3D models' accuracy and the calculation results of the tomato canopy were analyzed and evaluated.

### 2.3. Building multi-visual image data acquisition platform

For overcoming the problems of single camera image such as the small amount of collected data in a single time, the poor, timeliness, and be difficult to meet the needs of efficient and high-precision collection of crop data in complex agricultural fields. In this study, a multi-source tomato canopy 3D data synchronous acquisition system was constructed based on Kinect2.0 sensors. Compared with the binocular acquisition system, the system realized high precision and comprehensive acquisition of crop structure characteristics and had high adaptability for crop information acquisition in the outdoor environment.

The system consisted of three Kinect2.0 sensors, laptops, coils, and camera brackets. Each Kinect2.0 sensor was installed in a fixed position of the adjustable angle shooting frame. The three Kinect 2.0 sensors were placed at an angle of 120 degrees and connected to the laptop through an adapter with USB3.0. The Kinect sensor sent the near-infrared light pulse to the target continuously. Then received the near-infrared light pulse returned from the object by the photosensitive module. The target distance was obtained by detecting the flight round-trip time of the pulse, and the spatial position information of the tomato canopy was dynamically obtained. The effective acquisition range of depth data was from 0.5 m to 4.5 m, and the error accuracy was about 2 ~ 6 mm.

This system could collect accurate and stable point cloud and color image information of the tomato canopy in a short time. To ensure the growth of tomato plants, data acquisition work was carried out in an outdoor environment. The schematic diagram of the 3D synchronous acquisition platform for the tomato canopy is in Fig. 2:

### 2.4. Experimental collection method

The Kinect 2.0 sensors were assembled with an adjustable height tripod to ensure that the tomato canopy was displayed in the center of the image. In the process of data acquisition, Perspective 1 was the central perspective which has grayscale test card correction in the image, and the other two perspectives were Perspective 2 and Perspective 3 according to counterclockwise rotation. The canopy morphology images of tomato canopy at 20d (initial flowering stage, June 12), 30 d (florescence, June 22), and 40 d (primary fruit stage, July 3) were obtained by the acquisition platform.

To obtain the phenotypic traits of the tomato plant, manual measurement and image scanning were carried out in the outdoor environment. Image scanning refers to acquiring the multi-view color image and 3D point cloud data of the tomato canopy. Manual measurement mainly measured plant height, canopy width, and leafstalk angle using the ruler, vernier caliper, and the electronic angler on the day before or after the image information acquisition, which was used to verify the validity of calculated results. The images of the tomato canopy are shown in Fig. 3.

For reducing the influence of environmental factors on tomato canopy imaging, horizontal shooting was adopted to obtain image information on the tomato canopy. The whole data acquisition cycle was approximately 30 days.

### 3. Calculation principles and methods

The distribution of point clouds in 3D space was discrete for the

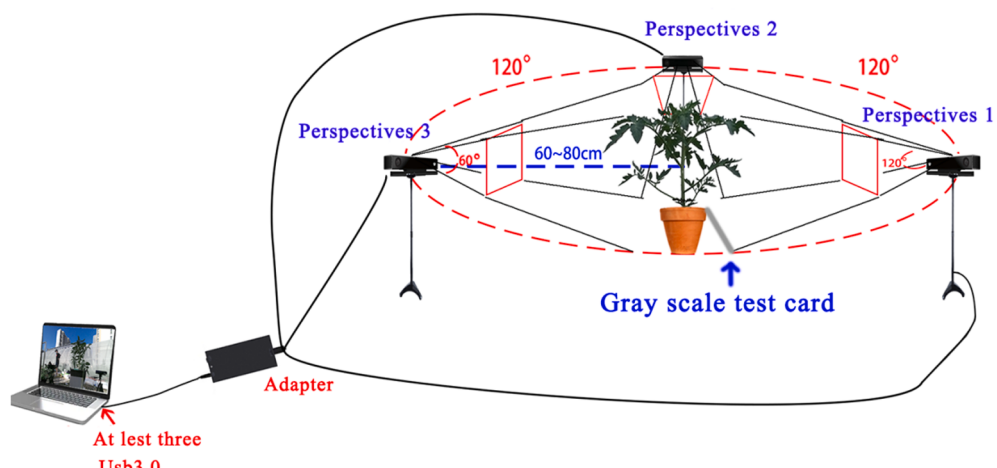


**Fig. 2.** The 3D data synchronous acquisition platform of tomato canopy.

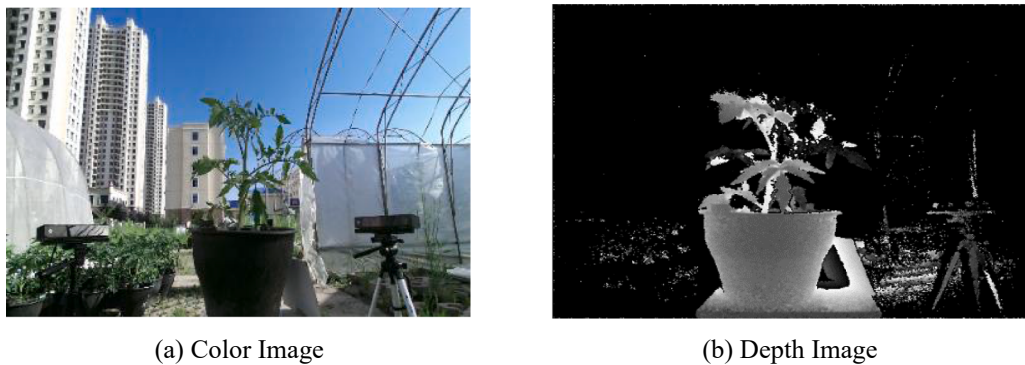


**Fig. 3.** Image acquisition of tomato canopy.

tomato canopy, and its complex 3D canopy morphology and spatial coordinates were not defined by a certain law or a specific numerical relationship. Thus, the establishment of the position relationship between 3D cloud points was the greatest difficulty. For the depth image and color image of the tomato canopy obtained by the Kinect 2.0 sensor, the 3D coordinate mapping relationship between the color image and the depth image was established through the mapping function of the Kinect 2.0 sensor. Each point of the tomato canopy after image information mapping registration contained 3D coordinates ( $x, y, z$ ) and color attributes (R, G, B). In addition, there was a redundant background point cloud and a specific amount of noise in the original images, which had a certain influence on the spatial position and 3D structure of the tomato canopy. Therefore, the 3D point cloud preprocessing included the following two steps:

First, considering the low weight of the redundant background point cloud and canopy structure in the original images, conditional filtering was used to remove the invalid background information and improve the importance of the point cloud.

Second, aiming at the problems of noise, outliers, and holes in the tomato canopy's point cloud. The SOR filtering algorithm was used to remove canopy noise and improve the measurement accuracy and characteristic recognition speed of the canopy.

Through the above pretreatment steps, the accurate point cloud was obtained with a clear canopy structure without aggregation outliers or heterochromatic points.

### 3.1. Preprocessing of 3D point cloud for the tomato canopy

#### 3.1.1. Conditional filter

When 3D point cloud information of the tomato canopy was acquired by the Kinect 2.0 sensor, as well as background noise and mottled points. Conditional filtering was used to eliminate those points according to the points' conventional attributes. The coordinate's conditional constraints were performed by using Eq. (1) to extract the target canopy point cloud from the single-perspective original point cloud.

$$\begin{cases} X_d \leq x \leq X_u \\ Y_d \leq y \leq Y_u \\ Z_d \leq z \leq Z_u \end{cases} \quad (1)$$

where  $(X_d, X_u), (Y_d, Y_u)$ , and  $(Z_d, Z_u)$  represented the limited range of 3D Cartesian coordinates. Then according to each point's values of red, green, and blue (RGB) channels, the ultra-green index  $SG_i$  of each point was calculated (Du et al., 2021). The calculation Equation as shown in Eq. (2):

$$SG_i = \frac{G_i}{R_i + G_i + B_i} \quad (2)$$

The single perspective original point cloud was marked as  $R_i$ , and the tomato canopy point cloud was marked as  $T_i$ . And the conditional

filtered tomato canopy point cloud was marked as  $S_i$ . The filtering results as shown in Fig. 4:

According to the distribution of point clouds in the 3D Cartesian coordinate system, the spatial threshold ranges were set as  $[-0.5, 0.5]$ ,  $[0.6, 1.5]$ ,  $[-0.15, 0.6]$ , respectively. The original three perspectives point cloud was filtered according to Eq. (1) to obtain the canopy point cloud (Fig. 4 (b), 4 (e), and 4 (h)). In Fig. 4 (b), due to the recognition accuracy of the device and the influence of the background environment in the process of data acquisition, there were some noise point clouds with blue color in the tomato canopy's point cloud generated by the terminal equipment. This was invalid information for the tomato canopy point cloud, which came from the sky and greenhouse background. According to Eq. (2), each point's  $SG_i$  was calculated, and the conditional threshold  $\alpha$  of the  $SG_i$  was set to 0.5. Finally, the clearer tomato canopy's point cloud was obtained (Fig. 4 (c)).

There were still many near-range noise points and outliers around the leaves and tomato stem in the tomato canopy's point cloud. To further simplify the tomato canopy's point cloud and eliminate outliers and noise points, the SOR algorithm was selected to deal with discrete and isolated noises.

#### 3.1.2. SOR filter

The point clouds of the tomato canopy were usually unevenly spaced, resulting in many sparse outliers. It was assumed that each point in the point cloud data in the canopy space contained a certain amount of information. If the points in a region were denser, the information carried by the area was larger. This meant that the average point distance between points in an area within the tomato canopy point cloud was small. The noise information belonged to useless information, and the scattered average point distance was large in space. According to these characteristics, if the average distance from a point cloud to its adjacent point is greater than a certain threshold, the information expressed by these points could be ignored (Zhao et al., 2018).

SOR filtering performed  $k$  neighborhood statistical analysis on each point and calculated the average point distance from the point to its  $k$  neighbor points. SOR algorithm assumed that the obtained distance conformed to the Gaussian normal distribution, then the average point distance outside the set threshold could be defined as outlier and removed from the data set. The specific steps were as followed:

(1) Calculate the distance  $d_i$  from each point to its  $k$  neighbor points.

$$d_i = \sqrt{(x_0 - x_i)^2 + (y_0 - y_i)^2 + (z_0 - z_i)^2} \quad (3)$$

(2) Calculate the sum  $D$  of  $d_i$  and the average distance  $\mu$  from each point to its  $k$  nearest neighbors.

(3) Assume that the results conform to Gaussian distribution. Its shape was determined by  $\mu$  and standard deviation  $\sigma$ . The calculation of  $\sigma$  was as follows:

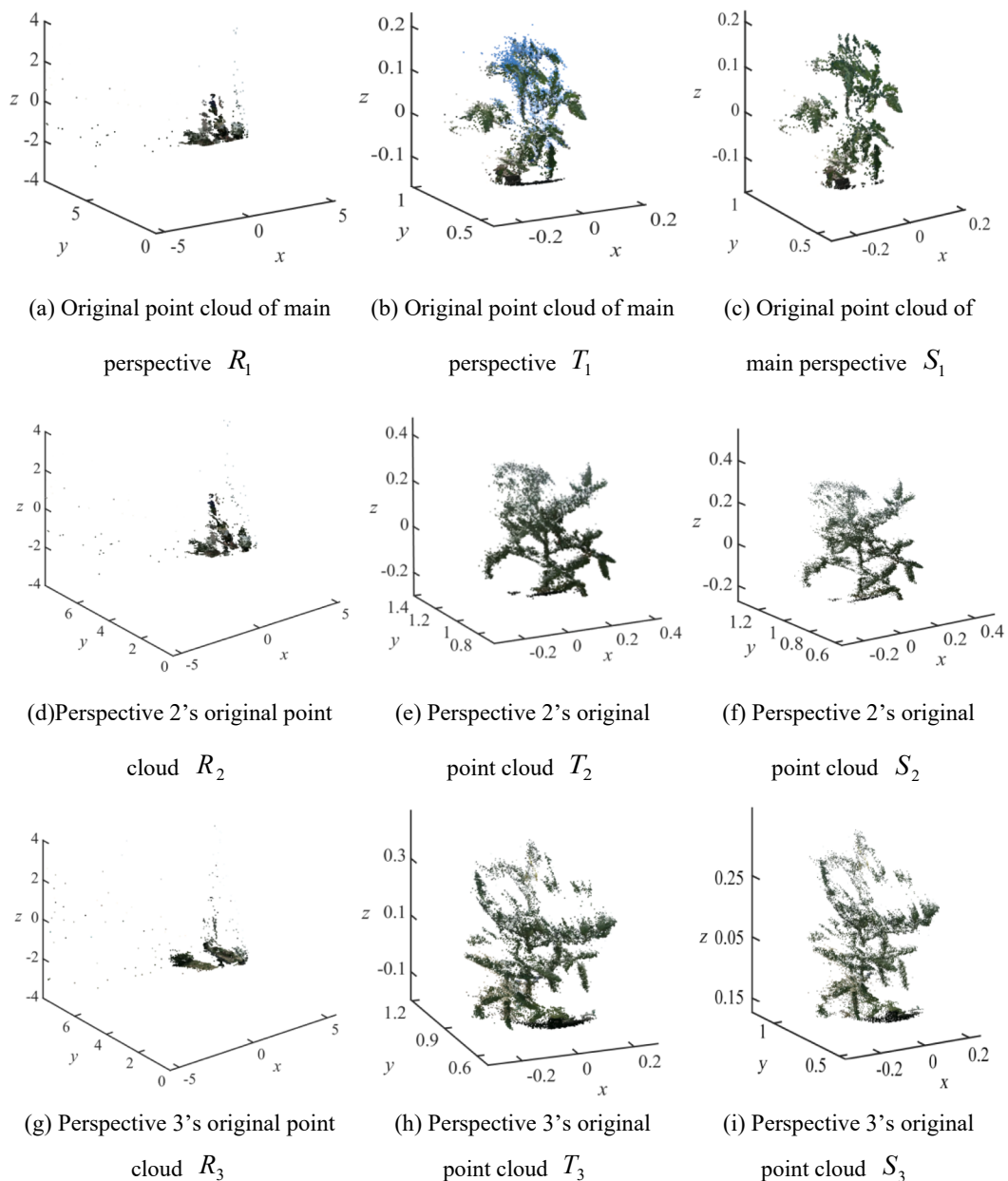


Fig. 4. Point cloud after Conditional Filter.

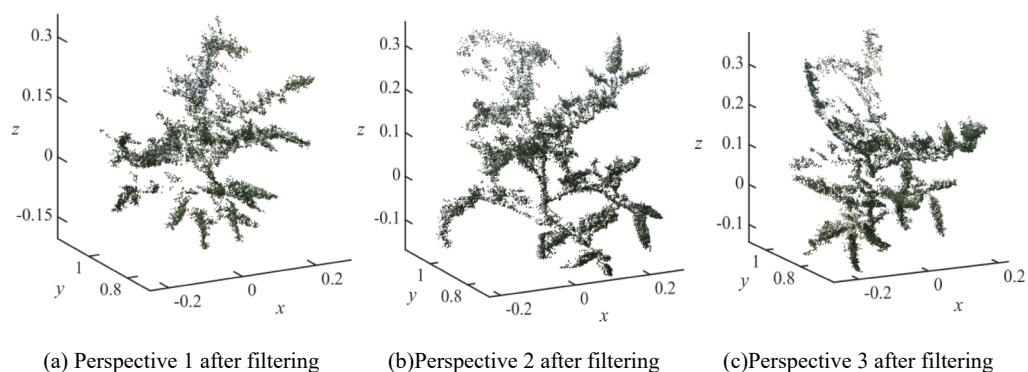


Fig. 5. Tomato canopy's point cloud after SOR Filter.

$$\sigma = \sqrt{\frac{\sum_{i=1}^k (d_i - \mu)^2}{k}} \quad (4)$$

- (4) Compare the  $\mu$  with the distance threshold  $d_t$ . Points whose  $\mu$  was greater than  $d_t$  were eliminated. The calculation method of  $d_t$  was as follows:

$$d_t = \mu + n^* \sigma \quad (5)$$

Where  $n$  was the arithmetic coefficient of distance standard deviation, the filtering results are shown in Fig. 5.

### 3.2. 3D point cloud registration of tomato canopy from multiple perspectives

The core of the registration of the multi-view 3D point cloud was to perform characteristic matching for multiple points that were not the same. The point cloud of perspective 1 was taken as the reference point cloud, and its point cloud spatial coordinate system was also set as the registration reference coordinate system. Point clouds of perspectives 2 and 3 were set to point clouds to be specified. The registration process was that the reference point cloud was gradually fused with the reference point cloud by rotating the reference point cloud, and all points in the point cloud were finally assigned to the same coordinate system of the point cloud (Zheng et al., 2021). To achieve efficient and accurate registration of multi-perspective point clouds, this study proposed a combination of the ISS algorithm with a high characteristic extraction rate and short iterative ICP algorithm to complete the rough registration of point clouds from two different perspectives. As a result, the initial spatial attitude of point clouds was corrected. Then, the high-speed and high-precision 3D-NDT algorithm was applied to accurately register the tomato canopy point cloud after rough registration. The registration process of multi-perspective 3D point clouds is shown in Fig. 6.

#### 3.2.1. Rough registration based on the ISS-ICP algorithm

The ISS algorithm addressed how to describe local features around each point in the tomato canopy's point cloud (Fu et al., 2021). The algorithm established a local coordinate system with the query point as the coordinate origin and calculated the covariance matrix and its eigenvalues of the neighborhood of the query point. Then the characteristic points were selected through the linear relationship between the eigenvalues. The selected characteristic points were used to describe the local feature information of the object, which was scaled invariant. In geometry, the eigenvalue and its corresponding eigenvector described an elliptic range, the eigenvector represented the main axis direction of the ellipse, and the eigenvalue represented the main axis length. Thus, the eigenvalues obtained from the covariance matrix and their corresponding eigenvectors described the local 3D shape of the point. The algorithm's flow chart is as shown in Fig. 7.

The equation of local domain covariance matrix  $p_{cov}$  centered at point  $p_i$  in this algorithm is shown as follows:

$$p_{cov} = \frac{\sum_{|p_i - p_j|} \left( \frac{(p_i - p_j)(p_i - p_j)^T}{r \parallel p_i - p_j \parallel} \right)}{\sum_{|p_i - p_j|} \left( r \parallel p_i - p_j \parallel \right)} \quad (6)$$

The eigenvalues  $\{\lambda_1^1, \lambda_2^1, \lambda_3^1\}$  of each point  $p_i$  were calculated  $\varepsilon_2$  according to the covariance matrix  $p_{cov}$  and arranged in descending order.  $p_{cov}$  was a positive definite matrix whose eigenvalue  $\lambda_i$  was nonnegative.  $\varepsilon_1$  was the threshold of  $\frac{\lambda_1^2}{\lambda_1^1}$ , and  $\varepsilon_2$  was the threshold of  $\frac{\lambda_2^3}{\lambda_1^1}$ , which were the basis for judging whether  $p_i$  was an approximate characteristic point. The extraction effect of characteristic points is shown in Fig. 8.

Fig. 8(a), 8(b), and 8(c) show the result after using the ISS algorithm to extract the contour characteristic of the point cloud. The tomato canopy structure had been greatly simplified. The contour structure of the canopy was more clearly visible, which would greatly reduce the time cost of the algorithm in subsequent registration operations.

Then, using a limited number of shorter iterations of the ICP algorithm (Shi et al., 2019), the rough registration of multi-perspective point clouds was sequentially performed to calculate the current optimal

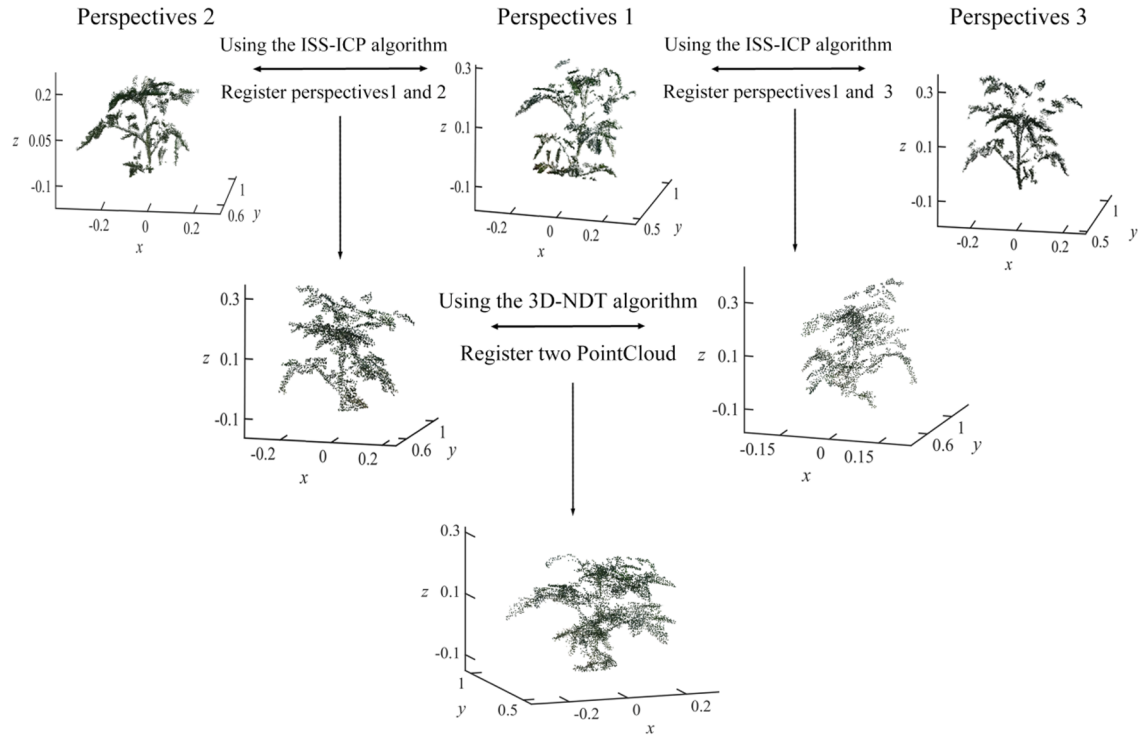


Fig. 6. Schematic diagram of the principle of point cloud registration.

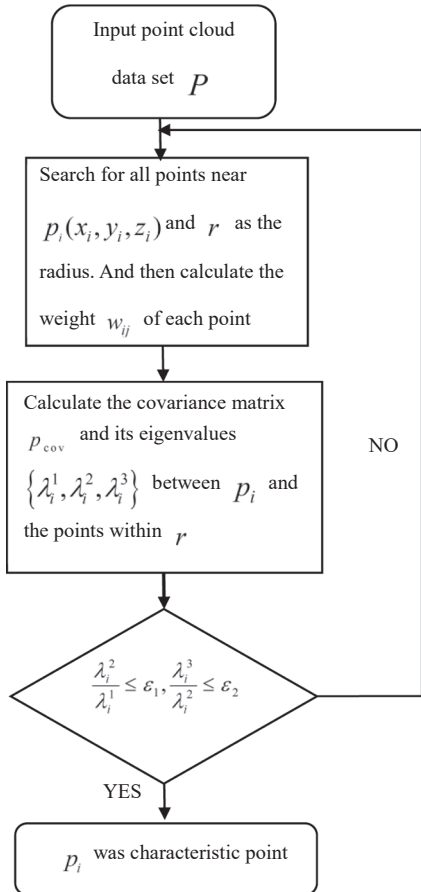


Fig. 7. The flow chart of ISS algorithm.

rotation translation matrix. The rough registration effect of

characteristic points is shown in Fig. 9.

Fig. 9 (a) shows the result of rotation and translation of the point cloud of perspective 2 with perspective 1 as the main perspective. Its point cloud and coordinate system were set as the reference point cloud and reference coordinate system. Fig. 9 ((b) shows the result of rotation and translation transformation of the point cloud of perspective 3. Compared with Fig. 8, the registration of the tomato canopy's point cloud model was relatively perfect without apparent fault and organ loss. Leaf morphology and stem structure were much clearer. The total number of per perspectives' point clouds was reduced to 16.67 % of the original ones on average, which would shorten the time-consuming of subsequent operations.

### 3.2.2. Accurate registration based on the 3D-NDT algorithm

After rough registration, the three-perspective tomato canopy's point cloud obtained a better initial pose. For further reducing the phase deviation to achieve rapid 3D reconstruction. The 3D-NDT algorithm was used for accurate registration based on rough registration. It was the generalization and improvement of NDT algorithm in 3D space, which could be applied to 3D point cloud (Yu et al., 2019), combining the normal distribution with standard optimal to determine the optimal registration of point cloud data. The algorithm flow chart is shown in Fig. 10:

In the 3D-NDT algorithm,  $p_i$  was any point of tomato canopy's point cloud  $P$ .  $T(\vec{\beta}, p_i)$  was a spatial transformation function, representing the mapping of  $p_i$  from the coordinate system of  $P$  to another tomato canopy's point cloud  $Q$  was a coordinate system. On the basis of the Euler angle method, the transformation parameter  $\vec{\beta}$  was represented by a 6-dimensional vector. The Equation of  $T(\vec{\beta}, p_i)$  was as follows:

$$\vec{\beta} = [t_x, t_y, t_z, \phi_x, \phi_y, \phi_z]^T \quad (7)$$

$$T(\vec{\beta}, p_i) = R_x R_y R_z p_i + \vec{t} \quad (8)$$

where  $t_x, t_y, t_z$  represented the translation amount of the corresponding

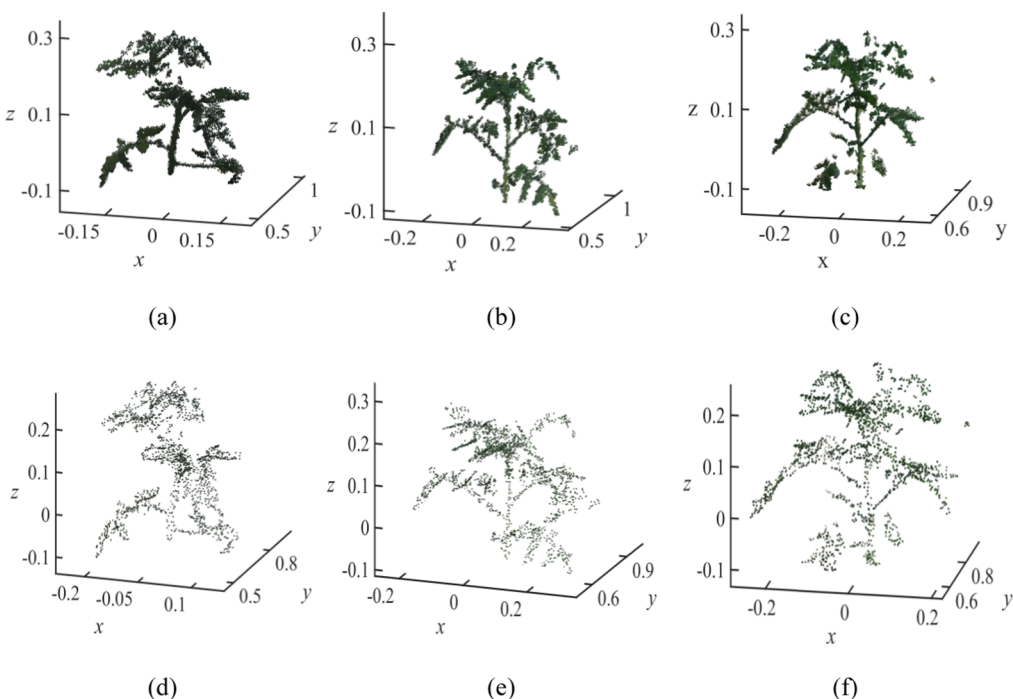
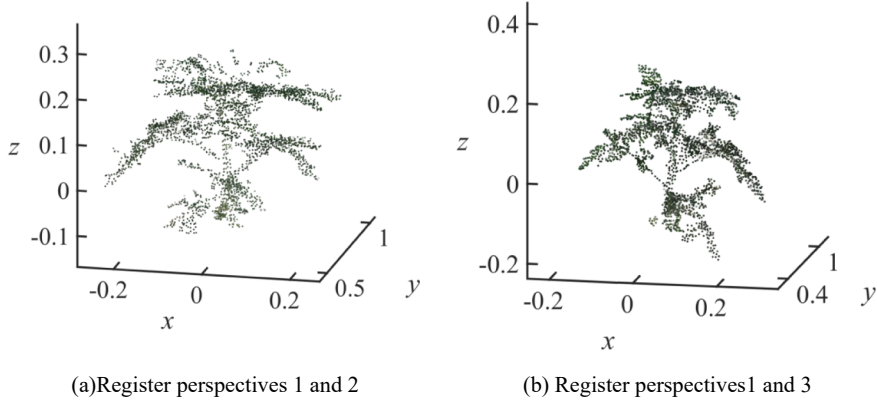
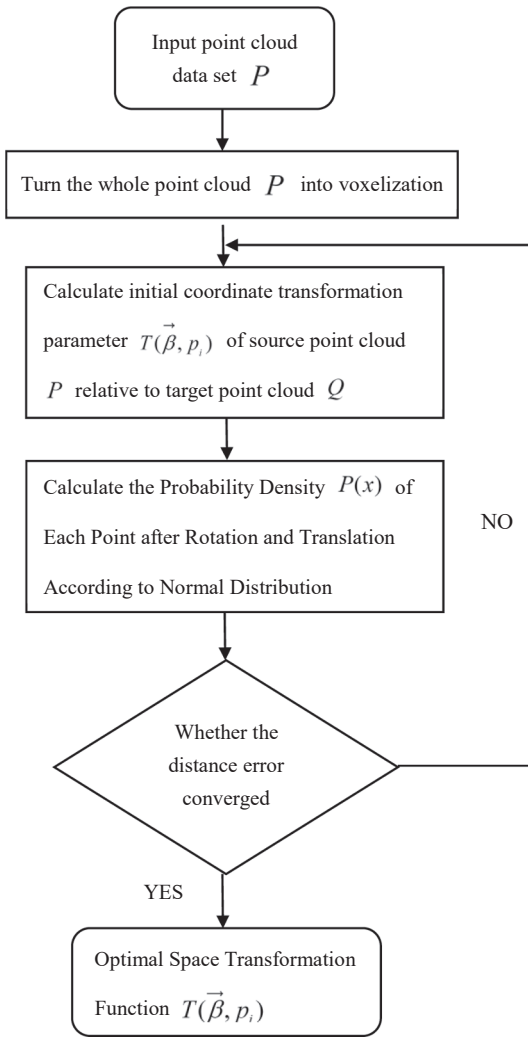


Fig. 8. Tomato canopy's point clouds and characteristic points from different perspectives (a) Original point cloud of perspective 1. (b) Original point cloud of perspective 2. (c) Original point cloud of perspective 3. (d) Characteristic point cloud of perspective 1. (e) Characteristic point cloud of perspective 2. (f) Characteristic point cloud of perspective 3.

**Fig. 9.** Rough registration of characteristic points.**Fig. 10.** The Flowchart of 3D-NDT algorithm.

point mapping from  $p_i$  to the target coordinate system, and  $\phi_x, \phi_y, \phi_z$  represented the rotation amount of the corresponding point mapping from  $p_i$  to the target coordinate system.  $R_x, R_y, R_z$  represented the rotation transformation of  $p_i$  from the carrier coordinate system to the reference coordinate system.  $\vec{t}$  represented the translation transformation of  $p_i$  from the carrier coordinate system to the reference coordinate system.  $\vec{a}$  represented the mean vector of the midpoint of the

voxelization. And  $cov_t$  represented the covariance matrix. The calculation Equations were as follows:

$$\vec{a} = \frac{1}{n} \sum_{i=1}^n p_i \quad (9)$$

$$cov_t = \frac{1}{n-1} \sum_{i=1}^n (x_i - \vec{a})(x_i - \vec{a})^T \quad (10)$$

$F(p_i)$  was the probability density function, which represented the probability density of each point  $p_i$  calculated according to the normal distribution. The calculation Equation of  $F(p_i)$  was as follows:

$$F(p_i) = \frac{1}{(2\pi)^{\frac{D}{2}} \sqrt{cov_t}} e^{-\frac{(p_i - \vec{a})^T cov_t^{-1} (p_i - \vec{a})}{2}} \quad (11)$$

The accurate registration results are shown in Fig. 11:

In Fig. 11(a) and 11(b), the final tomato canopy was obtained. The RMSE of Euclidean distance between registration point clouds was 0.0122. While in Fig. 11(c), the blue point cloud represented the point cloud shown in Fig. 9(a), and the green point was the point cloud shown in Fig. 9(b). According to the method of Section 2.1 and Section 2.2, the tomato canopy's point cloud collected from the three perspectives was pre-processed, roughly registered, and accurately registered. The tomato canopy's point cloud finally had a clear canopy structure and a good fusion distribution of stems and leaves. There were no interference factors, such as discrete aggregated leaf organs and random noise in the reconstructed canopy model, which could meet the accuracy requirements for subsequent calculation of phenotypic traits.

### 3.3. Calculation method of phenotypic traits for tomato canopy

#### 3.3.1. Contour detection of tomato canopy

Based on the above registration method, the reconstructed tomato canopy was obtained. In order to extract accurate canopy contour boundaries and reduce the error caused by point selection, the Alpha-Shape algorithm was used to obtain the edge contour of the tomato canopy from the 3D model (Liu et al., 2021b). By recording the rolling track of a common region circle, the ordered edge set of an object from an unordered point set was extracted to determine the boundary contour of the object (Dos Santos et al., 2018).

In this algorithm, the parameters that need to be manually set, included the circles' radiusr. Its unit was m, which determined the fineness of polyhedron generation. The tomato canopy model contour detection effect is shown in Fig. 12:

By using the AlphaShape contour extraction algorithm, the tomato canopy structure in 3D space was no longer presented as discrete points, and the fine discrete points of leaves were also aggregated to form a complete regular shape of the leaf pattern. The whole canopy skeleton

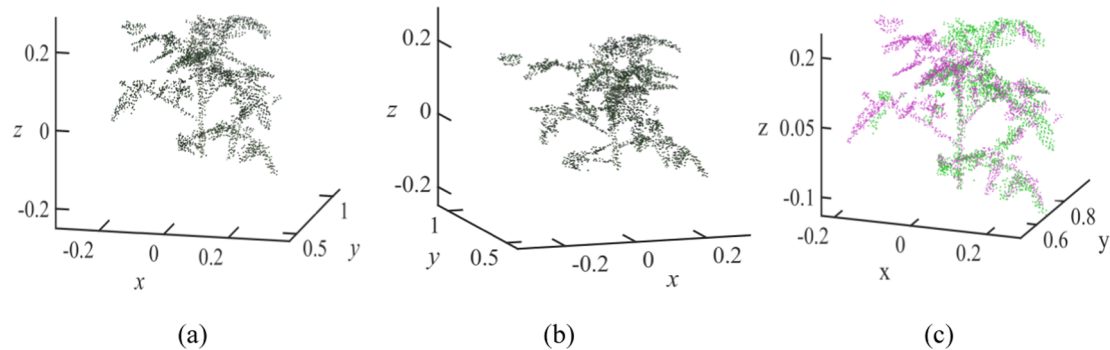


**Fig. 11.** The accurate registration results using the proposed algorithm. (a) Left rotation of canopy model by 45 degrees. (b) Right rotation of canopy model by 45 degrees. (c) Point cloud division of canopy model.

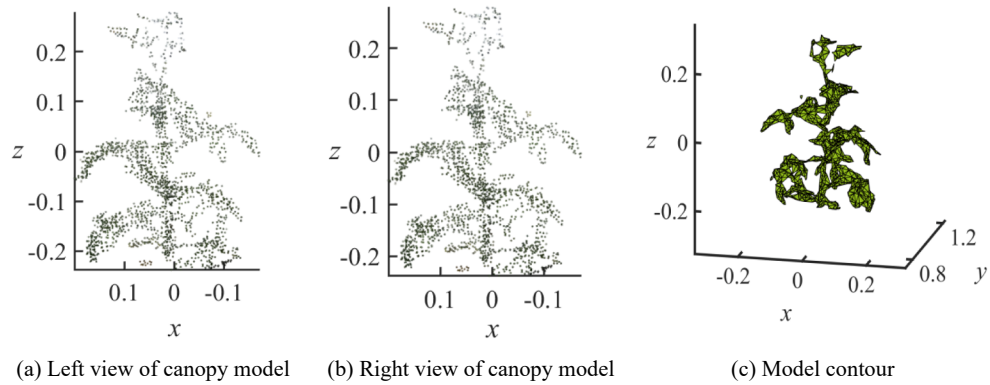


**Fig. 12.** Tomato canopy model and contour detection.

structure was further demonstrated to reduce the boundary error and improve the calculation accuracy for further calculation of phenotypic traits.

### 3.3.2. Calculation method of plant height

Plant height was one of the most basic indicators in the investigation of plant morphology and was defined as the distance between the plant base and the top of the main stem, namely the growth point of the main stem. It was one of the significant agronomic phenotypic traits of the tomato plants. During the whole stages of tomato planting, it was of great significance for tomato breeding and tomato yield estimation. On the basis of the contour extraction method introduced in Section 2.3.1, the plant height was calculated easily. Tomato canopy height calculation schematic diagram was as shown in Fig. 13:

In the Cartesian coordinate system, this study chose the direction from the  $xy$  plane and the direction perpendicular to the horizontal ground as the  $z$  axis. By obtaining the lowest and highest points of the center axis of the canopy, the vertical distance difference between the two planes was calculated according to the lowest and highest points found at the canopy height of tomato plants, namely tomato plant height  $h$  (Feng et al., 2019).

### 3.3.3. Calculation method of canopy width

The canopy width was an important parameter in tomato phenotype. The traditional method of measuring the canopy width was to measure the length of the east-west and north-south direction of the canopy and then calculate the average value. This method was intuitive and convenient, but the human cost was high. Because of the low resolution, the plant canopy image data obtained by satellite remote sensing image can only be used for large-area canopy extraction. It couldn't effectively extract the accurate single plant canopy. In this study, the 3D point cloud model of the tomato canopy was obtained and reconstructed by a

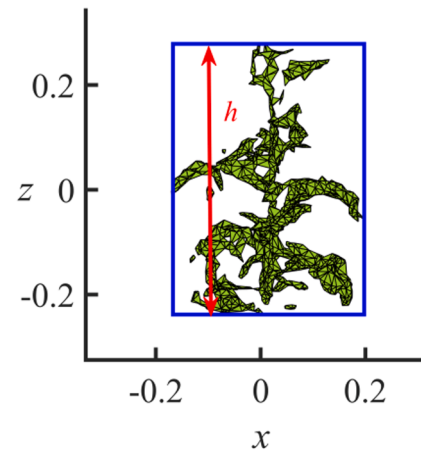


**Fig. 13.** Schematic diagram of plant height.

depth camera. The tomato canopy was calculated nondestructively, quickly, and accurately by 3D reconstruction technology, which could effectively overcome the above problems. In this study, the average value of the maximum canopy width in horizontal, vertical, and two directions of tomato canopy was used to represent the canopy width. The calculation schematic diagram of canopy width is shown in Fig. 14:

In Fig. 14, the edge detection method proposed in Section 2.3.1 was used to extract more accurate canopy edges. According to the agronomic requirements, the vertical distance between the transverse furthest point cloud of the canopy projected onto the ground was defined as the maximum length of the canopy, and the corresponding longitudinal distance was defined as the maximum width of the canopy. The average

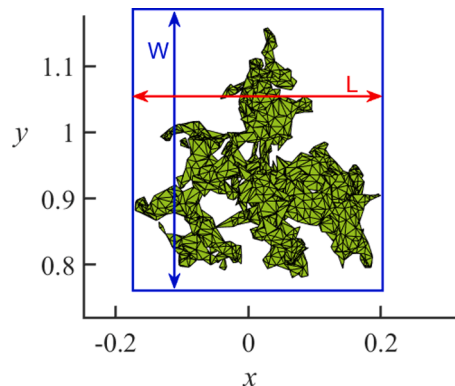


Fig. 14. Schematic diagram of canopy width.

value of the sum of the maximum length and the maximum width of the canopy was the canopy width. (Wang et al., 2022).

### 3.3.4. The extraction method of tomato canopy skeleton

The internal structure of the tomato canopy was complex, which was different from corn or soybean plants with a single main stem. The stem and leaves of tomato plants were seriously sheltered from each other, which made it difficult to extract crop skeleton structure and calculate leafstalk angle by using 2D images. However, the reconstructed 3D point cloud model of the tomato canopy could provide all-around canopy structure information compared with the 2D images. To accurately extract the stem skeleton structure of the living tomato plant, the improved density-based point cloud spatial clustering (DBSCAN) algorithm (Ferrara et al., 2018) was used. The algorithm flow chart is shown in Fig. 15:

The result of d clustering using DBSCAN algorithms is shown in

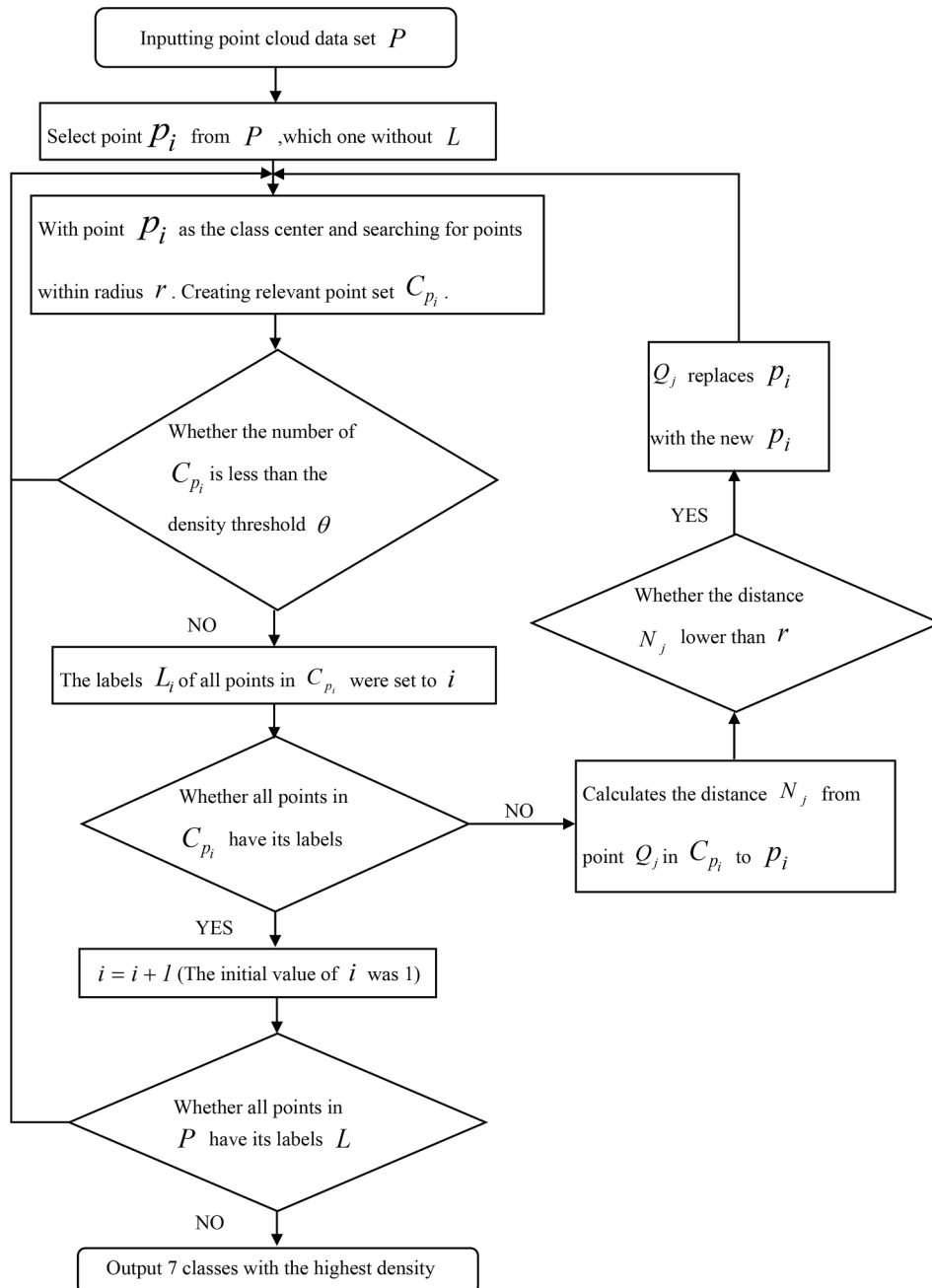


Fig. 15. Flowchart of DBSCAN algorithm.

**Fig. 16.**

**Fig. 16** (a) shows the clustering distribution of tomato canopy model after the DBSCAN algorithm. However, the density clustering algorithm, as an unsupervised algorithm, could just divide the clusters according to the density distribution, which was difficult to automate the separation of the leaves and stalks of crops. Therefore, based on the DBSCAN algorithm, the spatial distribution density of each cluster was calculated. By extracting the clusters with higher density among them, the automated segmentation of the stalks was realized. After that, the point cloud structure was obtained (**Fig. 16 (b)**). Meanwhile, there were still discrete leaf point clouds among the tomato canopy's point clouds, so the results in **Fig. 16(a)** were again processed by DBSCAN. The clustering division was shown in **Fig. 16(b)**. The orange part was the stem of the tomato plant. The algorithm was third performed on the extracted stem portions to obtain the cluster partitioning results (**Fig. 16(c)**). By traversing all cluster labels, the centroids  $C(x_c, y_c, z_c)$  of each cluster under the corresponding labels  $L$  were calculated. Combined with the method of Section 2.3.1, the extraction result of the stem node is as shown in **Fig. 17**:

**Fig. 17** shows the results of contour extraction by using the Alpha-Shape algorithm after the tomato canopy point cloud was extracted by the DBSCAN algorithm. The blue rhombus points represented leafstalk nodes, the red square points represented main stem nodes, and the main stem nodes were connected by black lines.

### 3.3.5. Calculation method of leafstalk angle

Leafstalk angle was one of the important traits constituting tomato canopy's phenotype. The leafstalk angle was the core to measure the canopy morphological structure, which directly affected the spatial distribution of crop canopy light and canopy morphology and was one of the main performance factors for estimating crop yield and population density (Miao et al., 2021; Zhang et al., 2021). Based on the 3D tomato canopy model, the optimal angle of view for observing a leafstalk angle could be found without limitation of the visual field. Combined with the extraction method of the tomato canopy skeleton proposed in Section 2.3.4, the calculation schematic diagram of the leafstalk angle is shown in **Fig. 18**:

Any main stem point  $A$  on a tomato plant and leafstalk on tomato plants and any endpoint  $B$  above  $A$  were connected to form line segments. The vertex  $A$  was associated with the endpoint  $C$  on the leafstalk to form a segmentc. At the same time, segment  $b$  was formed by endpoints  $B$  and  $C$ . And then, the leafstalk angle  $\theta$  was calculated based on the coordinate information of points  $A$ ,  $B$ , and  $C$  and the length of segments  $a$ ,  $b$ , and  $c$  (Zhu et al., 2019).

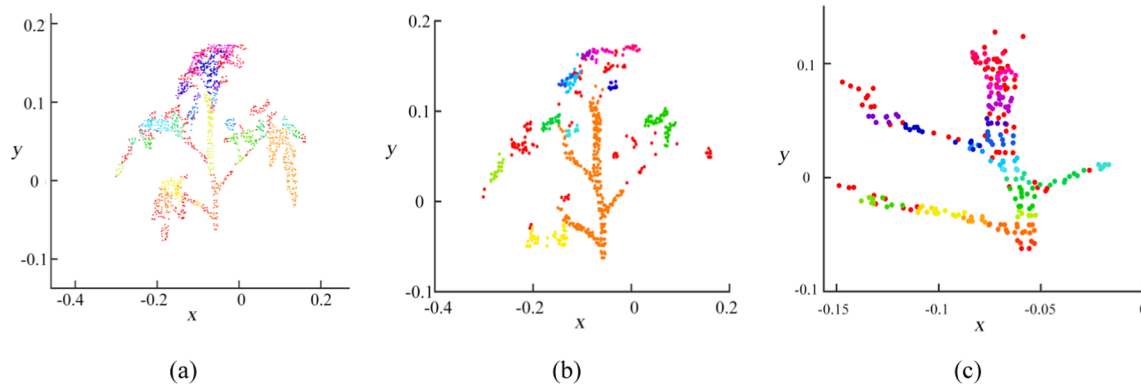


**Fig. 16.** The result of clustering. (a) Initial density clustering. (b) Twice density clustering after leaf separation. (c) Extraction of stem.

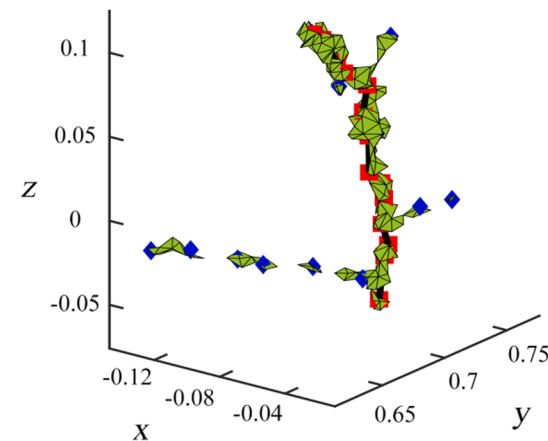


**Fig. 17.** Stem extraction result.

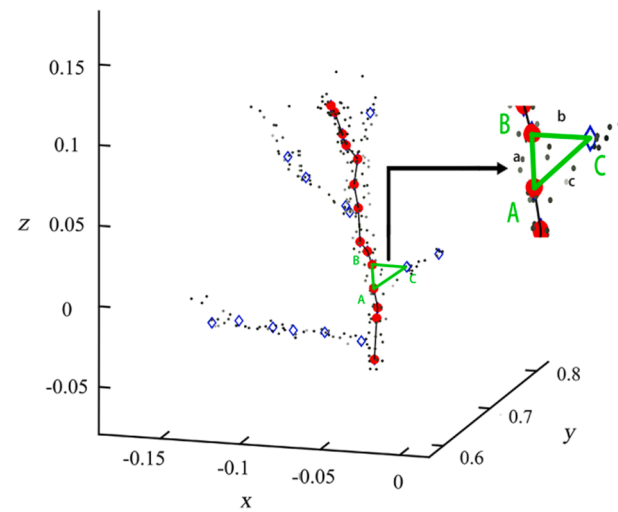


**Fig. 18.** Calculation Diagram of Leafstalk Angle.

## 4. Result analysis

### 4.1. Analysis of preprocessing results

In this study, denoising accuracy  $Q$  was used as the evaluation index to evaluate the performance and filtering effect of the conditional filtering algorithm, SOR filtering algorithm, and the quality of the final 3D point cloud of the tomato canopy.  $Q$  was calculated by counting 96 groups of point cloud data, such as the size of the original point cloud

and the number of noises removed by the algorithm. The calculation Equation was as follows:

$$Q = \frac{S_c}{S_t} \quad (12)$$

where  $S_c$  represented the number of outliers and noise removed,  $S_t$  indicated the total number of original point clouds in the tomato canopy. The change of three perspectives tomato canopy point cloud before and after conditional filtering are shown in Fig. 19.

Fig. 19(a), 19(c), and 19(e) showed the original data of tomato canopy collected from three perspectives. The area surrounded by a blue rectangle was the tomato canopy point cloud required for the study, and the other points were the background information that was unrelated to the canopy. After screening the 3D Cartesian coordinate threshold and the super-green numerical threshold set in Section 1.1 of this paper, the canopy point cloud was obtained (Fig. 19 (b), 19(d), and 19(f)).

The average filtering accuracy of this method was 91.7 %, which could accurately segment the required area in 3D space. However, it was difficult to deal with the near noise points on the edge and inside of the

target, so SOR filtering was needed to filter the noise points.

SOR filtering needed to artificially set two core parameters, namely the number of neighborhood points  $k$  and the standard deviation coefficient  $n$ , which could control the overall filtering effect.  $n$  could directly affect the tolerance of the SOR filter to noise. With the decreasing of  $k$  the filter would be more sensitive to recognize noise points, while increasing  $k$  would lead to the time complexity of the algorithm. Therefore, in order to find the adjustable parameters, filtering effect statistics on tomato canopy point cloud data was performed under different parameters. With different parameters, the change of the tomato canopy's point cloud before and after the SOR filtering is shown in Fig. 20.

In the study, the target point cloud of the tomato canopy accounted for a large proportion of the original data, and the weight of noise in the whole point cloud was small. As shown in Fig. 20(a1), there were 6060 close-range noise points in tomato stems, leaves, and canopy edges. In the case of setting the threshold  $k = 5$ ,  $n = 0.6$ , Fig. 20(a2) was obtained after SOR filtering. Totally, 555 noise points were removed, which means its  $Q$  was 9.15 %. In the case of setting the

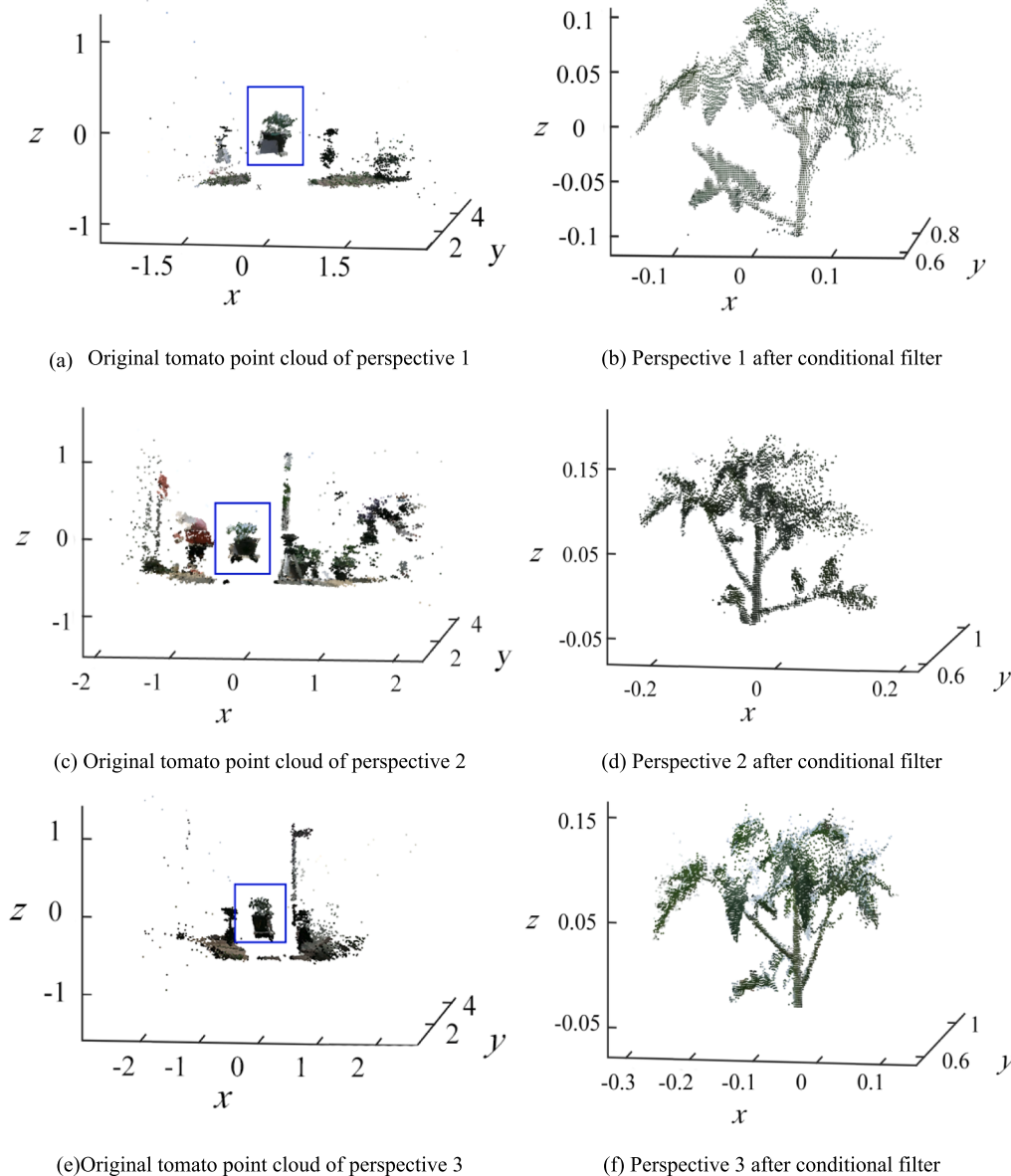


**Fig. 19.** Comparison of conditional filtering effect.

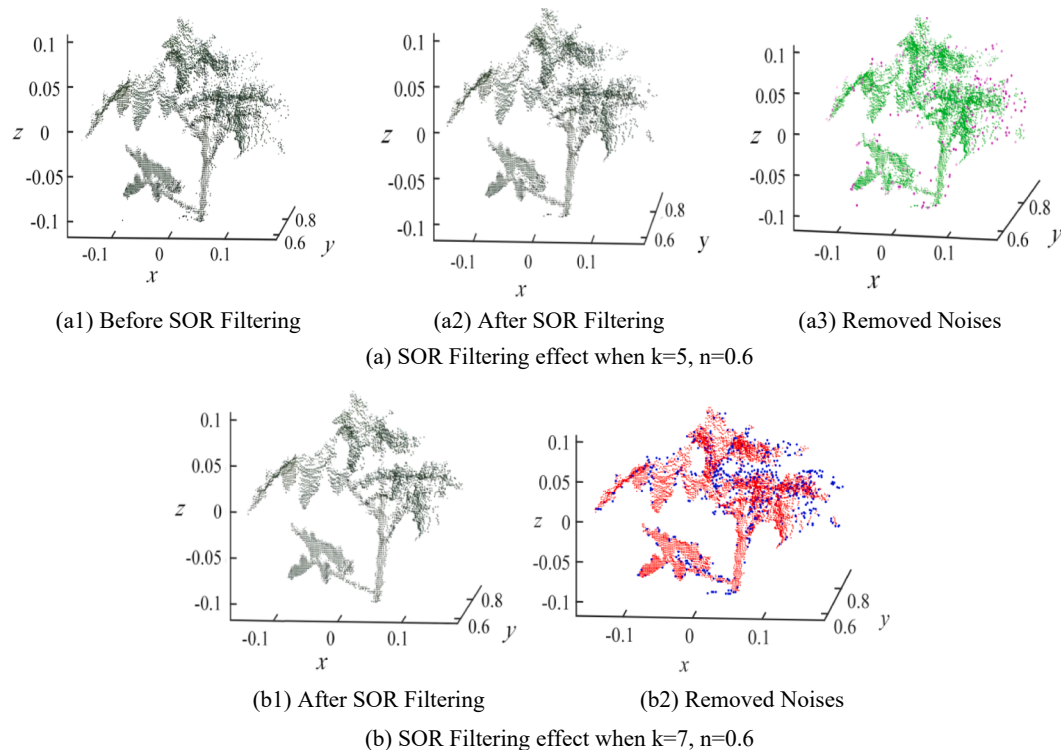


**Fig. 20.** SOR Filtering effects with different parameters.

threshold  $k = 7$ ,  $n = 0.6$ , Fig. 20(b1) was obtained after SOR filtering. 683 noise points were removed which means its  $Q$  was 11.27 %.

The green point cloud in Fig. 20(a3) and the red point cloud in Fig. 20 (b2) represented the filtered point clouds of tomato canopy structure by SOR algorithm. The blue points represented the outliers. From the visual effect evaluation, compared Fig. 20(a2) and 20(b1), only the increased  $k$  could remove more dense outliers. Part of the experimental results in the parameter setting experiment are shown in Table 2.

As shown in Table 2, the number of neighborhood points  $k$  was 7. The standard deviation coefficients were compared when  $n$  was 0.6 and 0.8, respectively. Since the coordinate unit of Euclidean distance was m, the automatic distance threshold  $d_t$  was sensitive to the change of  $n$ . Under the influence of high standard deviation coefficient, noise screening and division conditions were weaker, which led to the overall reduced denoising accuracy. It was difficult to remove relatively obvious outliers under the same number of neighborhood detection. Therefore,  $n = 0.6$  was chosen as a fixed standard deviation coefficient. On the other hand, under the same standard deviation coefficient, with the  $k$  increased, the denoising accuracy of the method was improved.

Compared Fig. 20(a3) with Fig. 20(b2), SOR filtering could

effectively remove the outliers of tomato canopy in the specified 3D canopy space and the complex distribution of noise points. The leaf tip, edge features, and stem details could be retained. At the same time, there was no apparent outlier noise in the point cloud of Fig. 20(b2). From the above data results, the SOR algorithm was an effective denoising method of the point cloud, which provided a more streamlined point cloud for initial registration by removing close-range outliers.

#### 4.2. Analysis of t registration results

##### 4.2.1. Analysis of rough registration effect based on ISS-ICP algorithm

The preprocessed tomato canopy's point cloud contained a clear canopy structure and leaves. However, for the registration of the multi-perspective point cloud, the cloud volume of the point cloud to be registered at this time was still relatively large, which increased the time cost of point cloud registration and affected the calculation accuracy of phenotypic traits. This would not meet the needs of precision agriculture for low time cost and high precision reconstruction of virtual plants. Thus, the ISS characteristic extraction algorithm was used to extract the tomato canopy's point cloud from different perspectives according to Eq. (6). The effect was shown in Fig. 21:

After the noise of the perspective1 was filtered by the algorithm, the number of point clouds was 5537. After down-sampling, 3723 points were left. After the ISS algorithm, 1970 point sets that could describe the contour shape of the whole point cloud were left. The number of point clouds was 5640 after the noise of perspective 2 was filtered by the algorithm. There were 3129 points left after down-sampling. There were 1140 point sets that could define the contour form of the entire point cloud after the ISS algorithm. While the number of point clouds was 6211 after the noise of perspective 3 was filtered by the algorithm in this work. There were 3265 points left after down-sampling, and following the ISS algorithm, there were 1557 points that could characterize the entire point cloud contour shape. Three characteristic point clouds were obtained by the ISS algorithm in Section 2.2.1, then the ICP algorithm was used to register the point cloud of the three perspectives point

**Table 2**  
SOR Filtering Denoising Effect with Different Coefficients.

Serial Number	Number	Neighborhood Number $k$	Threshold Coefficient $n$	The number of noise point	$Q$
CK1-3	6060	5	0.6	555	9.15 %
		7	0.6	683	11.27 %
		5	0.8	186	3.069 %
T1-3	6600	7	0.8	192	3.168 %
		5	0.6	547	8.28 %
		7	0.6	707	10.71 %
		5	0.8	376	5.69 %
		7	0.8	515	7.80 %

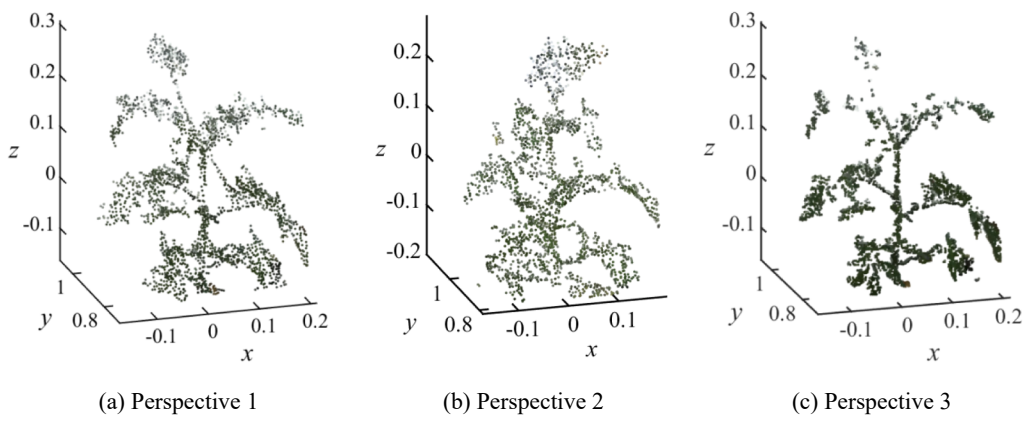


**Fig. 21.** Characteristic points set of tomato canopy's point cloud from different perspectives.

clouds. Finally, rotation and translation matrices were obtained. The registration results of two perspectives point clouds were shown in Fig. 22.

The above method could not only eliminate useless point pairs that couldn't represent the overall canopy contour in point cloud, but also obtain the optimal quaternion rotation and translation matrix. Finally, it reduced the initial point cloud to 28.37 %, 29.07 %, and 22.72 %, respectively, and effectively reduced the number of point clouds involved in registration.

#### 4.2.2. Analysis of accurate registration effect based on the 3D-NDT algorithm

For evaluating the effectiveness of the proposed algorithm in this study, it was compared with the traditional registration algorithm in terms of time cost and error. The registration effects of the proposed algorithm and the traditional algorithm are shown in Fig. 23, 24, and 25.

Fig. 23 shows the results of three-perspective registration by using the 3DNDT algorithm directly without rough registration. Fig. 24 shows the result of the ICP algorithm after rough registration. Fig. 25 shows the result of 3DNDT algorithm after rough registration.

In Fig. 23(c), the green part was the registration result of the tomato canopy point cloud collected by perspective 1 and the tomato canopy point cloud obtained by perspective 2. The purple part was the registration result of the tomato canopy's point cloud obtained by perspective 2 and the tomato canopy point cloud obtained by perspective 3. Fig. 23(c) shows that the plant canopy failed to get the correct fusion using only the 3DNDT algorithm, which just achieved the overlap of the main stem, but the leaves and stems inside the canopy were mismatched. This situation directly affected the calculation accuracy of phenotypic traits based on 3D tomato canopy.

In Fig. 24(c) the registration effect of the ICP algorithm was better than that of the NDT algorithm. A large part of the leaves was correctly registered and fused. This was because the ICP algorithm would calculate the Euclidean distance, covariance matrix, and rotation translation matrix of all points in the point cloud and another one in each iteration. Although the geometric characteristics of the tomato canopy's point cloud were fully utilized and preserved from the registration results, it was still being found that the canopy structure had a specific position offset. The results of the ICP algorithm still existed many discrete points without correct registration. In the subsequent study of phenotypic traits, the calculation of canopy width and plant height would cause greater interference.

In Fig. 25(a) and 25(b), the algorithm proposed here had a clearer tomato 3D canopy structure with higher registration accuracy and better visual effect. However, as shown in Fig. 25 (c), in the final point cloud fusion process, the down-sampling treatment caused a certain loss to the stem with a finer stem diameter at the top of the canopy.

For further verifying the effectiveness and superiority of the 3D reconstruction method of tomato canopy proposed in this study, the time cost and registration accuracy algorithms were compared in Table 3:

Combination 1 and combination 3 in Table 3 showed that the method proposed here realized fast registration compared with 3DNDT algorithm. The RMSE of the registration results decreased by 8.2041 %, and the registration error fluctuation range has a significant shrink tendency. The lower error limit was reduced by 26.33 % and the upper error limit was reduced by 10.71 %. Obviously, in Fig. 23(c) and 25(c), the method proposed here could reconstruct the tomato canopy more perfectly and stably. But the overall time consumption would increase due to the addition of the coarse registration operation of the front.

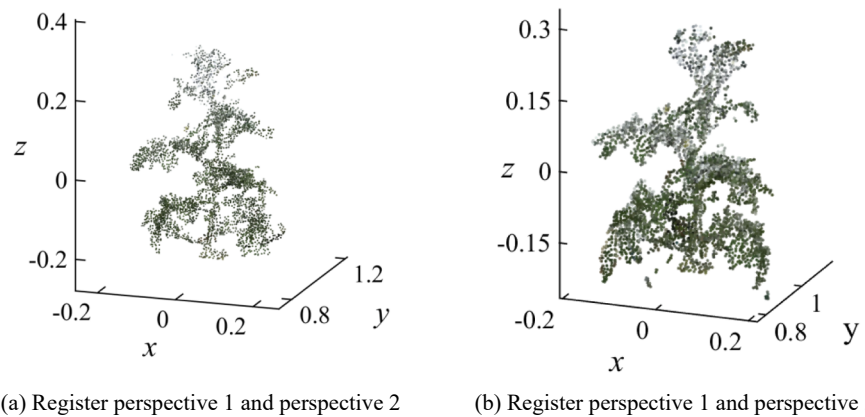


**Fig. 22.** Rough registration effect.

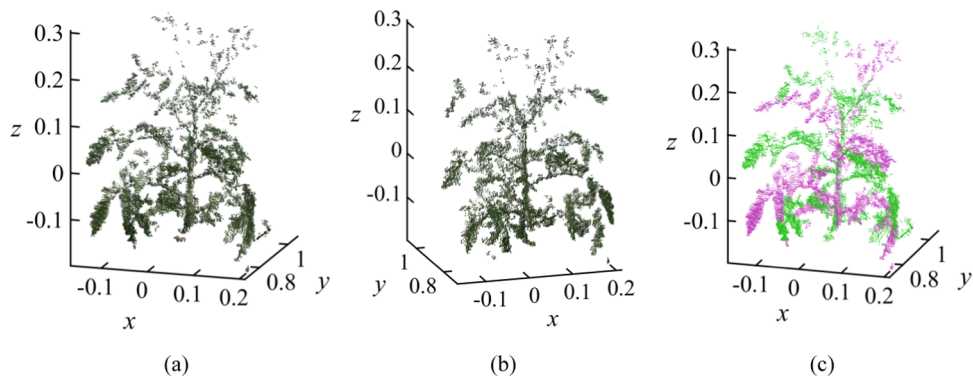


**Fig. 23.** Result of NDT algorithm. (a) Left rotation of canopy model by 45 degrees. (b) Right rotation of canopy model by 45 degrees. (c) Point cloud division of canopy model.

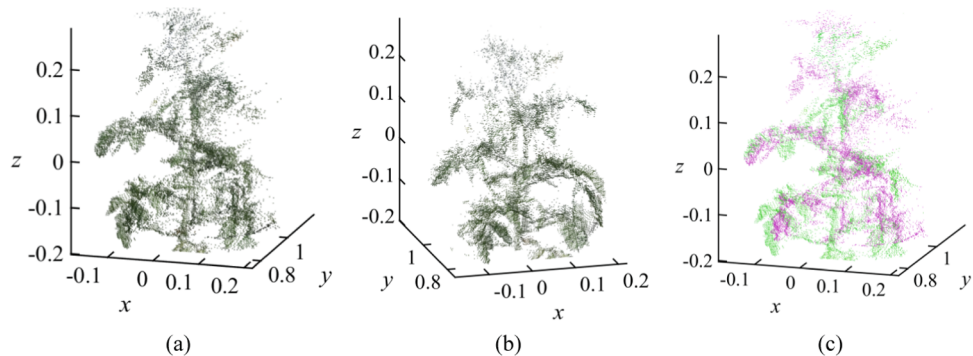


**Fig. 24.** Result of ICP algorithm (a) Left rotation of canopy model 45 degrees. (b) Right rotation of canopy model 45 degrees. (c) Point cloud division of canopy model.

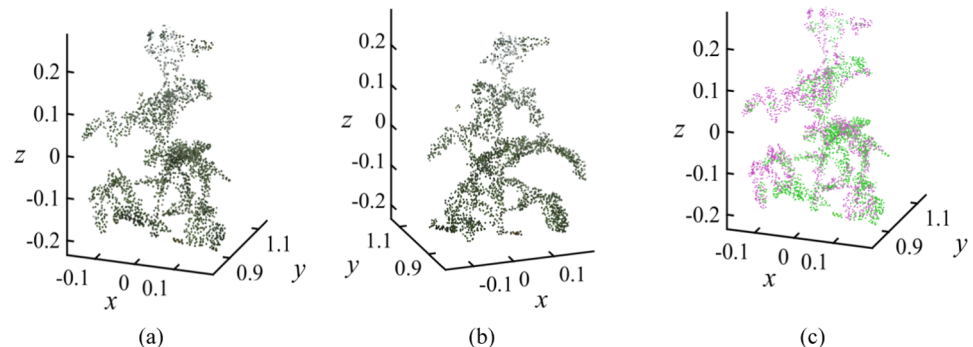


**Fig. 25.** Result of 3D-NDT algorithm based on ISS-ICP algorithm (a) Left rotation of canopy model by 45 degrees. (b) Right rotation of canopy model by 45 degrees. (c) Point cloud division of canopy model.

While compared with combination 1 and combination 2, the computational efficiency of the 3DNDT algorithm and the ICP algorithm in the accurate registration was improved by 73.7471 % on average when dealing with the same number of point clouds. Then the RMSE of registration was reduced by 68.8526 % on average. The error fluctuation range was decreased by 73.1681 %. As the number of point clouds to be registered increased, the proposed processing method had an obvious advantage over the ICP algorithm in terms of efficiency and error.

The proposed method further improved the robustness of the 3DNDT algorithm while taking into account the reconstruction speed and reducing the impact of data volume on the time complexity. It also had good adaptability to the streamlined point cloud with good robustness and fault tolerance for the noise and outliers in the point cloud. The overall computational efficiency and registration accuracy were much higher than those of ICP algorithms under the same conditions.

Moreover, the reconstructed canopy model was more observable with a clear structure, which could meet the demand for fast and accurate crop reconstruction. The method could be easily integrated with point cloud scanning devices on the same platform to meet the needs of real-time or near-real-time crop reconstruction.

#### 4.3. Calculation and analysis of phenotypic traits

##### 4.3.1. Calculation and analysis of plant height

To verify the effectiveness of the method, calculating plant height based on the reconstructed 3D canopy, the correlation between the calculated values and the measured values of plant height was analyzed. Based on the plant height calculation method proposed in Section 2.3.2, the plant height of the reconstructed tomato canopy structure model was calculated. At the same time, the three-perspective canopy point cloud

**Table 3**

Time cost and registration accuracy of algorithms.

Combination Number	Rough Registration	Accurate Registration	Total Points Number	Total Points	Time Cost of Rough Registration/S	Time Cost of Accurate Registration/S	Total Time Cost/S	RMSE
1	ISS-ICP	3DNDT	16,128	3752	27.9117	24.0714	24.0714	0.0422
			15,508	3128	26.0144	22.3195	22.3195	0.0340
			15,340	3765	25.2173	21.9912	21.9912	0.0339
			9648	2409	19.1167	15.5763	15.5763	0.0302
			8163	1821	18.1713	14.8293	14.8293	0.0256
			7982	1807	18.1843	12.0941	12.0941	0.0301
			7919	1833	17.4133	13.1740	13.1740	0.0224
			7467	1688	16.0698	11.7057	11.7057	0.0332
			5768	1235	12.9447	10.4041	10.4041	0.0246
2	ISS-ICP	ICP	16,128	3752	27.9117	97.1174	125.0291	0.1551
			15,508	3128	26.0144	72.5476	98.5620	0.1320
			15,340	3765	25.2173	77.9733	103.1906	0.1132
			9648	2409	19.1167	56.5066	75.6233	0.0657
			8163	1821	18.1713	44.0809	62.2522	0.0652
			7982	1807	18.1843	40.6697	58.8540	0.0981
			7919	1833	17.4133	46.5642	63.9775	0.0961
			7467	1688	16.0698	32.4035	48.4733	0.0623
			5768	1235	12.9447	24.0017	36.9464	0.0743
3	–	3DNDT	16,128	–	–	24.0714	24.0714	0.0422
			15,508	–	–	22.3195	22.3195	0.0340
			15,340	–	–	21.9912	21.9912	0.0339
			9648	–	–	15.5763	15.5763	0.0302
			8163	–	–	14.8293	14.8293	0.0256
			7982	–	–	12.0941	12.0941	0.0301
			7919	–	–	13.1740	13.1740	0.0224
			7467	–	–	11.7057	11.7057	0.0332
			5768	–	–	10.4041	10.4041	0.0246

after conditional filtering was used to calculate the plant height in the same way. The calculated values of two methods were compared with the measured values. In order to reduce measurement error, the same tomato plant in the horizontal direction from five different perspectives was measured to acquire the average value.

The calculation error of plant height according to the calculated data and measured data is shown in Fig. 26.

In Fig. 26, compared with the measured data, the overall error range of the calculated data was 0.0824 cm ~ 1.9797 cm, the average error was 0.4372 cm, and the RMSE was 0.6120. The calculation error was caused by the inevitable error due to the influence of environmental and human factors in the process of manual measurement. In addition, device accuracy for the top stem would have a certain edge distortion. However, compared with manual measurement data and Single perspective tomato canopy point clouds, the overall error range was from 0.2108 cm to 5.6137 cm, the average error was 1.3818 cm, and the RMSE was 1.1396. The result showed the value of plant height calculated using a single perspective point cloud led to a certain error, which was hard to meet the agronomic needs for rapid and accurate characterization of crop phenotypes.

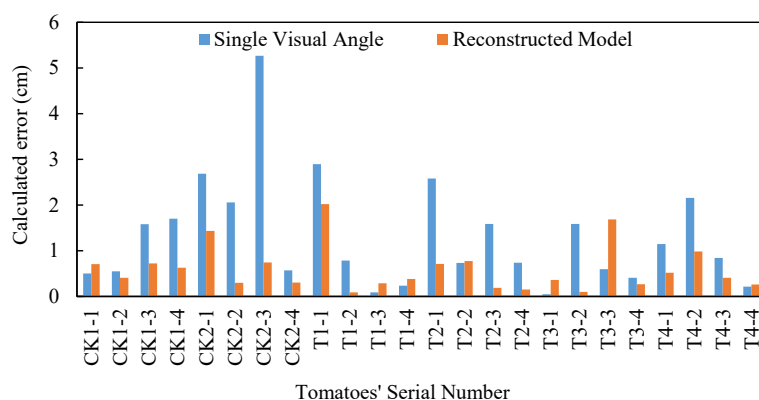
Thus, the calculation method of plant height based on a well-round 3D model of a tomato canopy achieved a good result with an error of 4 %.

In order to further verify the effectiveness of the calculation method of plant height, the linear correlation between the calculated and measured plant height of the tomato canopy model was established, as shown in Fig. 27:

In Fig. 27, the determination coefficient  $R^2$  between the calculated values and measured values was 0.961. According to the fitting line expression equation, the regression coefficient and regression intercept were between 1.047 and 0.014, which indicated that the plant height calculated based on the reconstructed 3D tomato canopy model was closely related to the measured values. And it has also proved the effectiveness of 3D reconstruction algorithms of tomato canopy.

#### 4.3.2. Calculation and analysis of canopy width

In order to verify the effectiveness of the calculation method of canopy width based on the 3D tomato canopy, the correlation between the calculated values and the measured values were established. Then the effectiveness of the proposed calculation method of canopy width

**Fig. 26.** Calculation error of plant height.

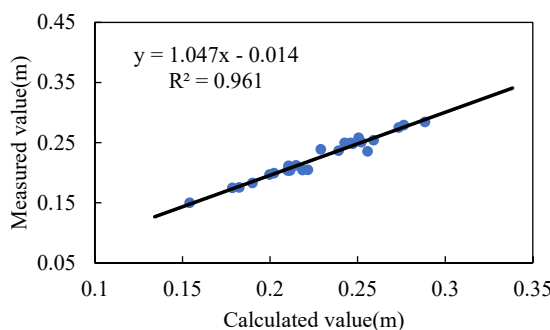


**Fig. 27.** The correlation of plant height between the calculated and the measured values.

was evaluated. The calculation error of canopy width according to the calculated data and measured data is shown in Fig. 28:

In Fig. 28, the overall error range was from 0.2585 cm to 4.9202 cm, the average error was 1.3633 cm, the standard deviation was 1.2644, and the RMSE was 1.1245. However, the overall error range of tomato canopy based on single-sided point cloud was 0.8108 cm ~ 7.4933 cm, the average error was 3.9281 cm, the standard deviation was 2.7426, and the RMSE was 1.6561. Due to the influence of artificial measurement and reconstruction operation, the distribution density of the leaf point cloud would change during the reconstruction process. The distribution of point clouds in the horizontal direction was enlarged or reduced to varying degrees. The correlation between the calculated values and the measured values is shown in Fig. 29:

In Fig. 29, the  $R^2$  between the calculated value and the measured value of canopy width was 0.809. According to the fitting line expression equation, the regression coefficient and regression intercept were 0.9008 and 0.0457, respectively. There were specific slope differences and intercept differences with standard equation  $y = x$ , but the error was within the allowable range of high correlation. The calculation accuracy was 92.17 %, and the error rate was 7.83 %. The average error was 1.9273 cm, with a range from 0.0273 to 4.9171 cm. The canopy width's calculated value was closer to the actual tomato crown measurement, which proved the effectiveness of 3D reconstruction algorithms of tomato canopy.

#### 4.3.3. Calculation and analysis of leafstalk angle

To verify the validity of the reconstructed canopy structure model and the method of calculating leafstalk angle based on the skeleton extraction method, the correlation between the calculated values and the measured values of leafstalk angle was established. And the calculation error of the leafstalk angle according to the calculated data and measured data is shown in Fig. 30.

The  $R^2$  between the calculated value and the measured value of the leafstalk angle shown in Fig. 30 was 0.922, which indicated that the method of calculating the phenotypic parameters of the tomato canopy

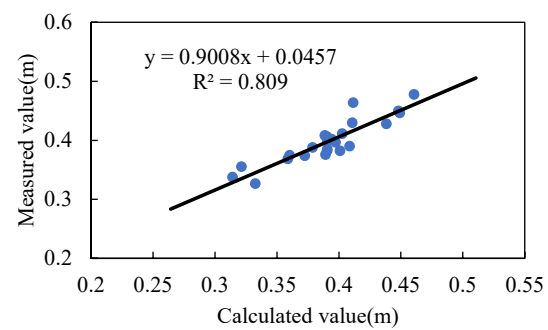


**Fig. 29.** The correlation of canopy width between the calculated and the measured values.

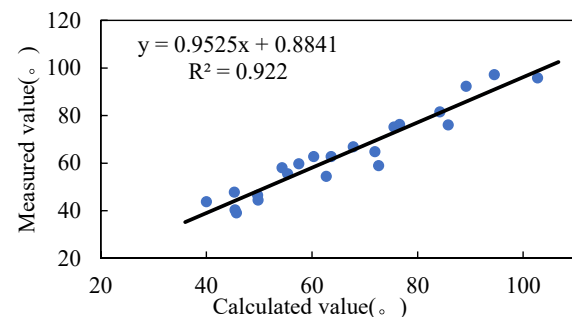


**Fig. 30.** The correlation of leafstalk angle between the calculated and the measured values.

leafstalk angle through the reconstructed tomato canopy structure model was scientific and adaptable. According to the fitting line expression Equation, the regression coefficient and regression intercept were 0.9525 and 0.8841, respectively. There were small slope differences and intercept differences with the standard equation  $y = x$ , but the error was within the allowable range of high correlation. The error range was  $0.5^\circ \sim 11.6^\circ$ , and the average calculation error was  $5.17^\circ$ . The main reason for the error was limited by the minimum recognition accuracy of the hardware shooting device. In addition, there was an artificial error in the traditional manual measurement, which would cause some damage to the overall canopy morphology structure, making the data different before and after the second acquisition. In summary, based on the reconstructed tomato canopy structure model, the structural skeleton of the tomato canopy was extracted. The calculation accuracy was 91.76 %, and the error rate was 8.24 %.

## 5. Discussion

### 5.1. Reconstruction strategy

In this study, a multi-perspective system was constructed with three Kinect 2.0 sensors to achieve the 3D reconstruction of the tomato canopy at initial flowering stage, florescence, and primary fruit stage. On this basis, the tomato canopy's phenotypic traits were calculated accurately.

The 3D reconstruction of tomato plants was a crucial part of the calculation of the phenotypic traits, and there was also a large number of interfering factors in the 3D point cloud data obtained from either single or multiple perspectives. The conditional filtering and SOR filtering methods used in this study could better achieve the target segmentation and data smoothness of the canopy of a single crop. For the canopy segmentation of group plants, the method could only perform rough target extraction, and further improvement of the algorithm and parameter configuration was needed.

For large-scale unstructured group overlapping plant point clouds,

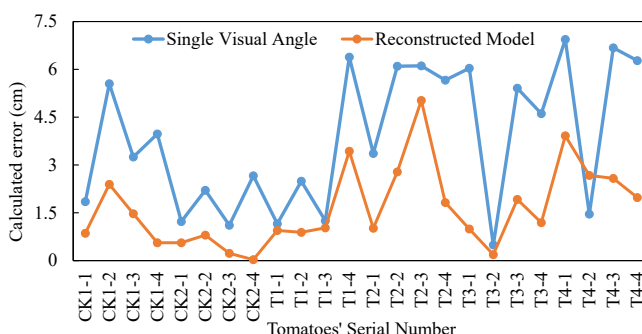


**Fig. 28.** Calculation error of canopy width.

the target detection can be achieved by using the Rand-LA network and voxelization (Chen et al., 2021; Zine-El-Abidine et al., 2021). Then, the filtering method in this study could be applied to eliminate the interference information in the data and provide a realistic and reliable point cloud for the 3D model reconstruction of plants. In terms of the large scanning devices currently applied to the acquisition of crop point cloud, although higher density point cloud data could be obtained, there were also a lot of redundant data and interference. On the premise of satisfying the accuracy of phenotypic calculation, according to the point cloud simplification criterion (maintaining the average curvature and geometric characteristics of the target), the adaptive curvature method, down-sampling method, and random sampling method can be used to simplify the point cloud, eliminate redundant data and retain effective crop information. Then, in the part of reconstruction, ISS, k-dimensional Tree ( $K_D$ -Tree), Sample consensus initial alignment (SAC-IA), et al. can be used to improve the 3D reconstruction quality of the canopy and speed up the algorithm execution (Ruchay et al., 2018; Yao et al., 2021; Liang et al., 2022).

For crops with irregular canopy structures, such as tomato and soybean plants, it had a large variability in point cloud density of stem and leaf organs. DBSCAN-based skeleton extraction method constructed here was applied to quickly delineate skeleton units and nodes, which achieved automatic extraction of skeleton internal corner points for calculation of phenotypic traits such as leafstalk angle and branch angle. If a smoother skeleton structure was needed from a large-scale dense point cloud, Laplace shrinkage, voxel grid shrinkage, B-sample curve could be combined with the skeleton extraction method in this study. Automatic detection of plant phenotypic traits such as leaf inclination and stem length could replace the traditional cumbersome and time-consuming manual measurement methods.

## 5.2. Experimental design and analysis

The experimental design of this paper was based on the effect of tillered onion on the growth index of tomato plants in each growth stage to construct a method for rapid characterization of the tomato physiological index. The tomato cultivation experiment was carried out in pots, which was not only beneficial to control the conditions of soil, fertilizer, and water, and to study the relationship between the changing trend of physiological indexes and the treatment of associated tillering onion as well as soil nutrient transformation, but also be helpful to study the automatic detection method of leaf area index, leaf inclination angle and projection area of tomato canopy which are difficult to be measured manually. So, the lack of mobile tomato phenotype detection technology and equipment in the field or greenhouse has been remedied.

In the case of other field crops, the pot method could accommodate large detection devices indoors for relevant experiments. This has facilitated the development of automated methods for phenotypic measurements of various field crops, enabling a non-invasive, high-throughput, all-around morph physiological phenotyping system for crop reproduction. The method also enabled systematic crop physiological phenotype collection in the near ground. It provided a reference solution for studying the trends of various physiological indicators and growth detection during the fertility cycle of field crops.

There were some shortcomings in the experiment. When using a point cloud acquisition device such as Kinect 2.0 sensor, irregular and heterochromatic noise clusters occurred in the target point cloud at the canopy edge due to background environmental factors. Therefore, the experiment requires further improvement in the data preprocessing algorithm to improve the detection accuracy of high-throughput phenotypes for dwarf plants. It was difficult to remove the noise using conditional filtering based on the distribution of color fields.

In terms of the outdoor experimental conditions, in order to ensure the reliability of data acquisition, the experiment should be carried out on a sunny day without wind as far as possible to avoid the influence of environmental factors.

## 5.3. Future work

In this study, a low-cost and high-precision multi-perspective 3D reconstruction technology of tomato plants were proposed based on Kinect 2.0 sensor. The current data acquisition in this paper used a static imaging approach. Data acquisition, model reconstruction, and extraction of phenotypic traits were realized in a relatively stable outdoor environment. And the manually measurable physiological indexes, including plant height, canopy width, and leafstalk angle were calculated in near real-time, and better calculation results were obtained. Thus, it replaced the traditional manual phenotypic measurement method. In future. On the one hand, the field platform for individual plants still needs improving. We will integrate the developed software platform and equipment on a movable platform, which will combine horizontal and vertical views for high-throughput crop point cloud acquisition, automatic segmentation of population crops, fruit recognition, etc. On the other hand, more detailed phenotypic traits will be obtained from the reconstructed crop canopy model. Combining light data from inside the tomato canopy at different growth stages and reconstructed model, a light distribution model may be developed to study the growth trends of tomato plants to determine the best phenotypic traits, which will improve the search for crop genotypes with accelerated growth or increased yield, provide a database for selection and breeding of suitable varieties.

## 6. Conclusion

The 3D reconstruction of the tomato canopy was achieved using the multi-view acquisition mode, and calculation methods were proposed for the non-destructive detection of phenotypic traits for the tomato canopy. The conclusions are as follows:

The conditional filtering and SOR filtering algorithm were used to filter and reduce the noise of tomato canopy's point cloud data. The ISS-ICP algorithm was used to quickly extract the characteristic point set representing the tomato canopy structure, which reduced the time complexity of the ICP algorithm and obtained a good initial point cloud pose quickly. The 3D-NDT algorithm based on voxel grid down sampling was used to accurately match the points, and the complete tomato canopy point cloud model was finally obtained. The average registration error of the proposed algorithm was 0.0214, smaller than that of the traditional NDT algorithm.

Based on the reconstructed tomato canopy model, the accuracy of plant height, canopy width, and leafstalk angle were 96.23 %, 95.17 %, and 91.76 %, respectively. The correlation coefficients  $R^2$  between the calculated values of plant height, canopy width, and leafstalk angle and the measured values were 0.9615, 0.809, and 0.9014, respectively. The results showed that the proposed algorithms could accurately and quickly calculate the phenotypic traits of the tomato canopy. The research results could provide technical support and reference for growth monitoring. It could also provide scientific cultivation and fine breeding of tomato plants.

## CRediT authorship contribution statement

**Tianyu Zhu:** Supervision, Writing - original draft. **Xiaodan Ma:** Conceptualization, Funding acquisition, Writing - review & editing. **Haiou Guan :** Conceptualization, Writing – review & editing, Supervision. **Xia Wu:** Resources, Funding acquisition. **Feiyi Wang:** Data Curation. **Chen Yang:** Data Curation. **Qiu Jiang:** Data Curation, Validation.

## Declaration of Competing Interest

The authors declare that they have no known competing financial interests or personal relationships that could have appeared to influence the work reported in this paper.

## Data availability

The data that has been used is confidential.

## Acknowledgments

Authors thank Haotian He, Miao Yu and Panpan Shen for their participation and contributions to the preliminary research. We thank Professor Fengjun Yang for his guiding suggestions in the design of tomato cultivation experiment. We thank Professor Yang Lu and Professor Jinming Liu for their work in English editing and grammar proofreading of this paper.

## Funding

This study was funded jointly by the National Natural Science Foundation of China (funding code: 31601220 and 31801905), the Natural Science Foundation of Heilongjiang Province, China (funding codes: LH2021C062, LH2020C080 and LH2021C066), and the Heilongjiang Bayi Agricultural University Support Program for San Heng San Zong, China (funding codes: TDJH202101 and ZRCQC202006).

## References

- Burgess, A.J., Renata, R., Tiara, H., Murchie, E.H., 2017. Exploring relationships between canopy architecture, light distribution, and photosynthesis in contrasting rice genotypes using 3d canopy reconstruction. *Front. Plant Sci.* 8, 734. <https://doi.org/10.3389/fpls.2017.00734>.
- Caruso, L., Russo, R., Savino, S., 2017. Microsoft Kinect V2 vision system in a manufacturing application. *Rob. Comput. Integrat. Manuf.* 48, 174–181. <https://doi.org/10.1016/j.rcim.2017.04.001>.
- Chen, Y., Xiong, Y., Zhang, B., Zhou, J., Zhang, Q., 2021. 3D point cloud semantic segmentation toward large-scale unstructured agricultural scene classification. *Comput. Electron. Agric.* 190, 106445 <https://doi.org/10.1016/j.compag.2021.106445>.
- Condotta, I.C., Brown-Brandl, T.M., Pitla, S.K., Stinn, J.P., Silva-Miranda, K.O., 2020. Evaluation of low-cost depth cameras for agricultural applications. *Comput. Electron. Agric.* 173, 105394 <https://doi.org/10.1016/j.compag.2020.105394>.
- Da Silva, D., Han, L., Costes, E., 2014. Light interception efficiency of apple trees: a multiscale computational study based on MAppleT. *Ecol. Model.* 290, 45–53. <https://doi.org/10.1016/j.ecolmodel.2013.12.001>.
- Dong, Q., Wang, Y., Yang, L., Yang, W., Shi, Q., Xu, Y., 2010. Parameter extraction and simulation of tomato three-dimensional morphological structure. *Trans. Chin. Soc. Agric. Eng.* 26 (14), 38–42. <https://doi.org/10.3969/j.issn.1002-6819.2010.z2.008>.
- Dos Santos, R.C., Galo, M., Carrilho, A.C., 2018. Building Boundary Extraction From Lidar Data Using a Local Estimated Parameter For Alpha Shape Algorithm. *Int. Arch. Photogramm., Remote Sens. Spatial Inform. Sci.* 42 (1), 127–132. <https://doi.org/10.5194/isprs-archives-XLII-1-127-2018>.
- Du, J., Fan, J., Wang, C., Lu, X., Zhang, Y., Wen, W., Liao, S., Yang, X., Guo, X., Zhao, C., 2021. Greenhouse-based vegetable high-throughput phenotyping platform and trait evaluation for large-scale lettuces. *Comput. Electron. Agric.* 186, 106193.
- Feng, J., Ma, X., Guan, H., Zhu, K., Yu, S., 2019. Calculation method of soybean plant height based on depth information. *Acta Opt. Sin.* 39 (05), 258–268. <https://doi.org/10.3788/AOS201939.0515003>.
- Ferrara, R., Virdis, S.G., Ventura, A., Ghisu, T., Duce, P., Pellizzaro, G., 2018. An automated approach for wood-leaf separation from terrestrial LiDAR point clouds using the density based clustering algorithm DBSCAN. *Agric. For. Meteorol.* 262, 434–444. <https://doi.org/10.1016/j.agrformet.2018.04.008>.
- Forero, M.G., Murcia, H.F., Méndez, D., Betancourt-Lozano, J., 2022. LiDAR Platform for Acquisition of 3D Plant Phenotyping Database. *Plants* 11 (17), 2199. <https://doi.org/10.3390/plants11172199>.
- Fu, R., Xian, C., Li, G., Wan, J., Cao, C., Yang, C., Gao, Y., 2021. Rapid 3D reconstruction of bean plants for accurate phenotypic identification. *J. Zhejiang Univ. (Science Edition)*, 48 (05), 531–539. Doi: 10.3785/j.issn.1008-9497.2021.05.002.
- Gao, M., Yang, F., Wei, H., Liu, X., 2022. Individual Maize Location and Height Estimation in Field from UAV-Borne LiDAR and RGB Images. *Remote Sens.* (Basel) 14 (10), 2292. <https://doi.org/10.3390/rs14102292>.
- Guan, H., Zhu, K., Feng, J., Ma, X., Yu, S., 2019. Registering feature points for multi-source images of soybean canopies. *J. China Agric. Univ.* 24 (2), 145–153. <https://doi.org/10.1184/j.issn.1007-4333.2019.02.16>.
- Huo, X.L., Zhu, C.C., Jiang, H., Yuan, Q., Wang, J.J., Wang, J.Y., et al., 2021. Rapid profiling of IAA and SA in tomato fruit during ripening using low-cost paper-based electroanalytical devices. *Postharvest Biol. Technol.* 180, 111635 <https://doi.org/10.1016/j.postharvbio.2021.111635>.
- Li, X., Zeng, J., Wang, H., Xu, L., 2019. Design and real-time imaging technology of three-dimensional scanning LiDAR, 503004–0503004(8). Infrared and Laser Engineering 48 (5). <https://doi.org/10.3788/irla201948.0503004>.
- Li, X., Ding, Q., Chen, X., He, R., Wang, X., Li, P., 2020a. Parameterization of 3D Topological Phenotypes of Wheat Root Architecture in Field Populations. *J. Jiangsu Agric.* 36 (4), 936–941. <https://doi.org/10.3969/j.issn.1000-4440.2020.04.018>.
- Li, Z., Guo, R., Li, M., Chen, Y., Li, G., 2020b. A review of computer vision technologies for plant phenotyping. *Comput. Electron. Agric.* 176, 105672 <https://doi.org/10.1016/j.compag.2020.105672>.
- Liang, P., Lin, W., Luo, G., Zhang, C., 2022. Research of hand-eye system with 3D vision towards flexible assembly application. *Electronics* 11 (3), 354. <https://doi.org/10.3390/electronics11030354>.
- Liu, F., Hu, P., Zheng, B., Duan, T., Zhu, B., Guo, Y., 2021a. A field-based high-throughput method for acquiring canopy architecture using unmanned aerial vehicle images. *Agric. For. Meteorol.* 296, 108231 <https://doi.org/10.1016/j.agrformet.2020.108231>.
- Liu, X., Wang, Y., Feng, K., Yang, Y., Zheng, Y., 2021b. Canopy Parameter Estimation of Citrus grandis var. Longyanus Based on LiDAR 3D Point Clouds. *Remote Sens.* 13 (9) <https://doi.org/10.3390/rs13091859>.
- Miao, T., Zhu, C., Xu, T., Yang, T., Li, N., Zhou, Y., Deng, H., 2021. Automatic stem-leaf segmentation of maize shoots using three-dimensional point cloud. *Comput. Electron. Agric.* 187, 106310 <https://doi.org/10.1016/j.compag.2021.106310>.
- Rose, J.C., Paulus, S., Kuhlmann, H., 2015. Accuracy analysis of a multi-view stereo approach for phenotyping of tomato plants at the organ level. *Sensors* 15 (5), 9651–9665. <https://doi.org/10.3390/s150509651>.
- Rouzbeh Kargar, A., MacKenzie, R., Asner, G.P., van Aardt, J., 2019. A Density-Based Approach for Leaf Area Index Assessment in a Complex Forest Environment Using a Terrestrial Laser Scanner. *Remote Sens. (Basel)* 11 (15), 1791.
- Ruchay, A., Dorofeev, K., Kober, A., 2018. An efficient detection of local features in depth maps. *Appl. Digital Image Proc. XLI* 1075223, 647–654. <https://doi.org/10.1117/12.2319913>.
- Schunck, D., Magistri, F., Rosu, R.A., Cornelissen, A., Chebrolu, N., Paulus, S., Léon, J., Behnke, S., Stachniss, C., Kuhlmann, H., Klingbeil, L., Agudo, A., 2021. Pheno4D: A spatio-temporal dataset of maize and tomato plant point clouds for phenotyping and advanced plant analysis. *PLoS One* 16 (8), e0256340.
- Shi, X., Peng, J., Li, J., Yan, P., Gong, H., 2019. The iterative closest point registration algorithm based on the normal distribution transformation. *Procedia Comput. Sci.* 147, 181–190. <https://doi.org/10.1016/j.procs.2019.01.219>.
- Shin, J., Hwang, I., Kim, D., Moon, T., Kim, J., Kang, W.H., Son, J.E., 2021. Evaluation of the light profile and carbon assimilation of tomato plants in greenhouses with respect to film diffuseness and regional solar radiation using ray-tracing simulation. *Agric. For. Meteorol.* 296, 108219 <https://doi.org/10.1016/j.agrformet.2020.108219>.
- Sun, G., Wang, X., Liu, J., Sun, Y., Ding, Y., Lu, W., 2019. Multimodal 3D reconstruction method of greenhouse tomato plants based on phase correlation. *Trans. Chin. Soc. Agric. Eng.* 35 (18), 134–142. <https://doi.org/10.11975/j.issn.1002-6819.2019.18.017>.
- Wang, F., Ma, X., Liu, M., Wei, B., 2022. Three-Dimensional Reconstruction of Soybean Canopy Based on Multivision Technology for Calculation of Phenotypic Traits. *Agronomy* 12 (3), 692. <https://doi.org/10.3390/agronomy12030692>.
- Wu, X., Wu, F., Zhou, X., Fu, X., Tao, Y., Xu, W., Liu, S., 2016. Effects of intercropping with potato onion on the growth of tomato and rhizosphere alkaline phosphatase genes diversity. *Front. Plant Sci.* 7, 846. <https://doi.org/10.3389/fpls.2016.00846>.
- Yao, Z., Zhao, Q., Li, X., Bi, Q., 2021. Point cloud registration algorithm based on curvature feature similarity. *Measurement* 177, 109274. <https://doi.org/10.1016/j.measurement.2021.109274>.
- Yu, J., Chang, L., Fumiomi, Takeda., Elizabeth, A., Kramer., Hamid, Ashrafi., Jamal, Hunter., 2019. 3D point cloud data to quantitatively characterize size and shape of shrub crops, *Horticul. Res.* 6(1), 43. Doi: 10.1038/s41438-019-0123-9.
- Yu, H., Fu, Q., Sun, J., Wu, S., Chen, Y., 2019. Improved 3D-NDT point cloud registration algorithm for indoor mobile robots. *Chin. J. Sci. Instrum.* 40 (9), 151–161. <https://doi.org/10.19650/j.cnki.cjsi.1J905346>.
- Yuan, X., Zhao, C., Wen, W., Guo, X., Lu, S., Wei, X., 2012. Detailed Modeling of 3-D Configuration of Tomato Plant. *Trans. Chin. Soc. Agric. Machinery* 43 (12), 204–210. <https://doi.org/10.6041/j.issn.1000-1298.2012.12.037>.
- Zhang, Z., Ma, X., Guan, H., Zhu, K., Feng, J., Yu, S., 2021. A method for calculating the leaf inclination of soybean canopy based on 3D point clouds. *Int. J. Remote Sens.* 42 (15), 5719–5740. <https://doi.org/10.1080/01431161.2021.1930271>.
- Zhao, Y., Hu, Q., Li, H., Wang, S., Ai, M., 2018. Evaluating carbon sequestration and PM2.5 removal of urban street trees using mobile laser scanning data. *Remote Sens. (Basel)* 10 (11), 1759. <https://doi.org/10.3390/rs10111759>.
- Zhao, T., Nakano, A., Iwasaki, Y., 2021. Differences between ethylene emission characteristics of tomato cultivars in tomato production at plant factory. *J. Agric. Food Res.* 5, 100181 <https://doi.org/10.1016/j.jafcr.2021.100181>.
- Zheng, L., Wang, L., Wang, M., Ji, R., 2021. Automatic 3D point cloud reconstruction of Leaf lettuce based on Kinect camera. *Trans. Chin. Soc. Agric. Machinery* 52 (7), 159–168. <https://doi.org/10.6041/j.issn.1000-1298.2021.07.016>.
- Zhu, K., Ma, X., Guan, H., Feng, J., Zhang, Z., Yu, S., 2019. A method of calculating the leafstalk angle of the soybean canopy based on 3D point clouds. *Int. J. Remote Sens.* 42 (7) <https://doi.org/10.1080/01431161.2020.1854889>.
- Zhu, G.-Y., Sha, P.-F., Zhu, X.-X., Shi, X.-C., Shahriar, M., Zhou, Y.-D., Wang, S.-Y., Laborde, P., 2021. Application of melatonin for the control of food-borne *Bacillus species* in cherry tomatoes. *Postharvest Biol. Technol.* 181, 111656.
- Zine-El-Abidine, M., Dutagaci, H., Galopin, G., Rousseau, D., 2021. Assigning apples to individual trees in dense orchards using 3D colour point clouds. *Biosyst. Eng.* 209, 30–52. <https://doi.org/10.1016/j.biosystemseng.2021.06.015>.